Submitted to Physical Review

UCRL-18927
Preprint

RECEIVED
LAWRENCE
RADIATION LABORATORY

OCT 22 1969

LIBRARY AND
DOCUMENTS SECTION

# EXCITATION OF COLLECTIVE STATES IN LIGHT NUCLEI BY INELASTIC SCATTERING OF 20.3-MeV POLARIZED PROTONS

A. G. Blair, C. Glashausser, R. de Swiniarski,
J. Goudergues, R. Lombard, B. Mayer, J. Thirion,
and P. Vaganov

August 1969

AEC Contract No. W-7405-eng-48

TWO-WEEK LOAN COPY

*This is a Library Circulating Copy which may be borrowed for two weeks. For a personal retention copy, call Tech. Info. Division, Ext. 5545*

LAWRENCE RADIATION LABORATORY
UNIVERSITY of CALIFORNIA BERKELEY

UCRL-18927

## DISCLAIMER

This document was prepared as an account of work sponsored by the United States Government. While this document is believed to contain correct information, neither the United States Government nor any agency thereof, nor the Regents of the University of California, nor any of their employees, makes any warranty, express or implied, or assumes any legal responsibility for the accuracy, completeness, or usefulness of any information, apparatus, product, or process disclosed, or represents that its use would not infringe privately owned rights. Reference herein to any specific commercial product, process, or service by its trade name, trademark, manufacturer, or otherwise, does not necessarily constitute or imply its endorsement, recommendation, or favoring by the United States Government or any agency thereof, or the Regents of the University of California. The views and opinions of authors expressed herein do not necessarily state or reflect those of the United States Government or any agency thereof or the Regents of the University of California.

# EXCITATION OF COLLECTIVE STATES IN LIGHT NUCLEI BY INELASTIC SCATTERING OF 20.3-MeV POLARIZED PROTONS*

A. G. Blair

Los Alamos Scientific Laboratory,
University of California,
Los Alamos, New Mexico 87544

and

C. Glashausser† and R. de Swiniarski‡

Lawrence Radiation Laboratory,
University of California,
Berkeley, California 94720

and

J. Goudergues, R. Lombard, B. Mayer, and J. Thirion

Service de Physique Nucléaire à Moyenne Enérgie,
CEN-Saclay, Saclay, France

and

P. Vaganov

University of Leningrad,
Leningrad, U. S. S. R.

August 1969

*Work supported in part by the U. S. Atomic Energy Commission.

†Present address: Rutgers, The State University, New Brunswick, New Jersey.

‡NATO-Fulbright Fellow; permanent address: Institut des Sciences Nucléaires de Grenoble, France.

## ABSTRACT

Asymmetries and relative differential cross sections have been measured for elastic and inelastic scattering of 20.3 MeV polarized protons from light elements. The targets included $^{12}C$, $^{16}O$, $^{24}Mg$, $^{25}Mg$, $^{26}Mg$, $^{27}Al$, $^{28}Si$, and $^{40}Ca$. Significant differences have been observed in both the asymmetries and cross sections for transitions with a given angular-momentum transfer. The shapes of the asymmetries for $^{27}Al$ and $^{28}Si$ show some disagreement with the weak-coupling model prediction. Coupled-channels and DWBA calculations have been performed for the first $2^+$ and $4^+$ states in $^{24}Mg$ and $^{28}Si$, with several types of deformed spin-orbit potential. In principle it should be possible with a coupled-channels analysis to distinguish between vibrational and rotational models, and between positive and negative deformations. In fact, there are differences between the predictions of these models. However, none of them gives a good account of the $2^+$ and $4^+$ asymmetries in $^{24}Mg$ and $^{28}Si$ even when the full Thomas form of the spin-orbit potential is used. Microscopic- and macroscopic-model DWBA predictions of the $3_1^-$ and $5_1^-$ asymmetries in $^{40}Ca$ yield fair agreement with the experimental data.

# I. INTRODUCTION

Measurements of the asymmetry in the inelastic scattering of polarized protons from medium-weight nuclei have now been reported at 18.6,[1] 20.3,[2] 30,[3] 40,[4] and 49 MeV.[5] Results for some light nuclei at several energies have also been published.[6] Analyses of these data with the distorted-wave Born approximation (DWBA) or coupled-channel methods (CC) have been reasonably successful for collective levels. When the distortion of the full Thomas term is included in the interaction, the DWBA predictions for $2^+$ states in the Ni isotopes at 40 MeV, e.g., are very accurate.[7] Problems have appeared, however in attempts to describe the results with a microscopic model.[1,2] In the present paper, asymmetries are presented for inelastic proton scattering at 20.3 MeV from low-lying collective states in $^{12}C$, $^{16}O$, $^{24}Mg$, $^{25}Mg$, $^{26}Mg$, $^{27}Al$, $^{28}Si$ and $^{40}Ca$. A coupled-channels analysis of the data concentrates on $^{24}Mg$ and $^{28}Si$; predictions for $^{40}Ca$ are also shown. Results from an initial DWBA analysis of some of these data have already been published.[8]

The rotational model provides a reasonably accurate description of the low-lying levels of $^{24}Mg$ and $^{25}Mg$, but the neighboring nuclei in the s-d shell are not so well understood. A study of differential cross sections[9] for inelastic proton scattering in this region showed a marked transition between strong coupling for $^{25}Mg$ to weak coupling for $^{27}Al$. Deviations from the weak-coupling description could be revealed in differences in the asymmetries for the low-lying states in $^{27}Al$ and the first $2^+$ state in $^{28}Si$. The variations in the shapes of the asymmetries for a given orbital angular momentum transfer (L) are, in fact, generally interesting to study, since they indicate differences either in the structure of the states involved or in their mode of excitation.

Rotational and vibrational levels, e.g., may have different asymmetries. Provided the states can be simply described in terms of these macroscopic models, a coupled-channels analysis should adequately account for variations in the mode of excitation.

After a brief description of the experimental details in Sect. II, the measured asymmetries are presented and discussed in Sect. III. Parameters of the spherical optical-model potential for $^{24}Mg$ - $^{28}Si$ are given in Sect. IV. The results of a coupled-channels analysis of several inelastic transitions are also shown and discussed. The paper concludes with a short summary in Sect. V.

## II. EXPERIMENTAL METHODS

Details of the experimental arrangements have been described in Ref. 2. About 20 nA of 20.3 MeV polarized protons could generally be obtained on target at the Saclay sector-focused cyclotron with the external ionizer and trochoidal injection system.[10] The beam polarization was normally about 75%. Eight Si(Li) detectors were used to count the scattered protons; the over-all energy resolution in the eight systems was between 100 - 150 keV. The angular resolution was ± 2°. A carbon polarimeter continuously monitored the polarization of the incident beam. Two monitor counters placed above and below the beam line provided reliable normalization for relative cross-section measurements.

The purity and thickness of the targets used are listed in Table I. The magnesium targets were obtained from the Oak Ridge National Laboratory; the silicon and calcium targets were evaporated at the Saclay Laboratory. A Mylar target was used for the carbon and oxygen measurements.

## III. RESULTS

The measured differential asymmetries for many low-lying excited states in the nuclei studied in the present experiment are shown in Figs. 1-9. The cross sections for a few states are shown in later figures, but they are generally not illustrated since most are already available[9] at 17.5 MeV. The asymmetry is normalized to 100% beam polarization and is defined as follows:

$$A = \frac{1}{P_B} \frac{N_+ - N_-}{N_+ + N_-} \quad .$$

The quantity $P_B$ is the measured polarization of the beam; $N_+$ and $N_-$ are the yields of a given state for incoming protons with spin up and spin down, respectively. The Basel sign convention is followed.

The relative errors shown are generally purely statistical, unless peak separation or background subtraction was difficult, in which case the errors were increased appropriately. The use of a peak-stripping computer program allowed us to obtain results for several states which were not included in Ref. 8. The absolute error due to uncertainty in the calibration of the beam polarimeter is about ± 5%.

### A. The L=2 Transitions

#### 1. Even-even nuclei

Asymmetries for L=2 transitions in $^{24}$Mg, $^{26}$Mg, and $^{28}$Si are shown in Fig. 1. No two of the curves are precisely the same, and some of the variations are quite large. All, however, have two large peaks of positive asymmetry, with the possible exception of the 4.23-MeV state in $^{24}$Mg. The

data for the first $2^+$ ($2_1^+$) states in $^{24}Mg$ and $^{26}Mg$ are quite similar, but they are easily distinguishable from the $^{28}Si$ data by the large dip in the latter curve around 100°. The asymmetry for the second $2^+$ ($2_2^+$) state in $^{26}Mg$ at 2.94 MeV shows larger oscillations than any of the other curves. The results for the $2_2^+$ state in $^{24}Mg$ are scanty but even these show differences from the other data.

Considerable variations are also observed in the differential cross sections at this energy, as well as at 17.5 MeV,[9] 49.5 MeV,[11] and 55 MeV.[12] At 49.5 MeV, e.g., the relative cross sections for the two $2^+$ states in $^{24}Mg$ are quite different. At 55 MeV, the shape and yield of the $2_1^+$ states in $^{26}Mg$ and $^{28}Si$ are almost identical, but they are different from the results for the $^{24}Mg$ $2_1^+$ state. The cross section for the $2_2^+$ state in $^{26}Mg$ at 55 MeV deviates quite markedly from all these shapes. At the lower energies, 17.5 and 20.3 MeV, the cross section for the $2_1^+$ state in $^{26}Mg$ resembles that for the $^{24}Mg$ $2_1^+$ state more closely than that for the $^{28}Si$ $2_1^+$ state. The angular distributions of the $4_1^+$ states in $^{24}Mg$ and $^{28}Si$ are also very different. The 20.3-MeV data are generally consistent with the 17.5 MeV data, but there are some differences in details, particularly at large angles. For example, the angular distributions for the two $2^+$ states in $^{26}Mg$ are very similar to each other at 20.3 MeV, while at 17.5 MeV a rather large difference between the two appears around 120°.

Since the structure of the nuclei is changing rapidly in this region of the periodic table, it is probably not surprising to find the variations observed in passing from one nucleus to the next. While $^{24}Mg$ has a well-established rotational structure, the rotational structure of $^{26}Mg$ is not apparent.

Hartree-Fock calculations[13] of the ground-state of $^{28}$Si indicate that a spherical solution lies considerably higher in energy than a deformed solution, but the oblate and prolate solutions lie close together. At the time the present experiments and calculations were performed, the deformed nature of $^{28}$Si had not yet received extensive confirmation. Very recently, however, Alexander et al. measured[14] the quadropole moment of the $2_1^+$ state and determined that its shape is oblate. Bar Touv and Goswami[15] have also indicated that the rotational model can explain the energy levels and transition rates in the ground-state band of $^{28}$Si very nicely provided some mixing with the spherical state is allowed. They assumed, however, that the 4.97-MeV level in $^{28}$Si is the spherical 0+ state, and there is little experimental evidence to justify this assumption. Finally, differences in the $4_1^+$ cross sections for $^{24}$Mg and $^{28}$Si at 17.5 MeV have been explained[16] as due to a large positive hexadecapole moment in the ground state of $^{28}$Si; $^{24}$Mg was found to have a very small, and possibly negative, hexadecapole moment.

2. Odd nuclei

The weak-coupling model has been applied with considerable success to $^{27}$Al. This model provides a good explanation of the relative cross sections of the 0.842- ($1/2^+$), 1.013- ($3/2^+$), 2.212- ($7/2^+$), 2.731- ($5/2^+$), and 3.00-MeV ($9/2^+$) levels in $^{27}$Al and the $2_1^+$ state in $^{28}$Si at 1.77 MeV, observed, e.g., in (p,p'),[9] (d,d'),[17] and (e,e')[18] experiments. In its simplest form, all these $^{27}$Al levels except the $5/2^+$ states are supposed to arise simply from the coupling of a $d_{5/2}$ proton hole to the $2_1^+$ state in $^{28}$Si. The $5/2^+$ ground state and the 2.731-MeV $5/2^+$ state are orthogonal combinations of a $d_{5/2}$ hole coupled to the $0^+$ and the $2_1^+$ state. The wave functions of

these two $5/2^+$ states can then be written:

$$\psi_{gs} = (1-A^2)^{1/2}|0,5/2,5/2\rangle + A|2,5/2,5/2\rangle$$
$$\psi_{5/2+}{}^* = -A|0,5/2,5/2\rangle + (1-A^2)^{1/2}|2,5/2,5/2\rangle \quad . \tag{1}$$

The value of A has been determined[9] to be about 0.45.

With respect to the present data, the simple excited-core model predicts that the shapes of the differential asymmetries for the five excited states in $^{27}$Al should be the same as that for the $2_1^+$ state in $^{28}$Si. The data for $^{27}$Al are shown in Fig. 2. Note that the curves for the $1/2^+$, $3/2^+$ and $9/2^+$ states are very similar to each other and show the deep minimum at 100° characteristic of the $2_1^+$ state of $^{28}$Si. However, the $5/2^+$ and $7/2^+$ curves show variations from the simple prediction. Both these states were cleanly resolved from neighboring states, whereas the $1/2^+$ and $3/2^+$ levels were separated with difficulty. The $9/2^+$ level at 3.00 MeV could not be separated from the $3/2^+$ level at 2.976 MeV, but there is evidence from the 17.5 MeV work[9] that the cross section is due almost entirely to excitation of the $9/2^+$ state. The deviations thus do not seem to be experimental in origin and should be ascribed to a failure of the simple model.

The model has not, in fact, been able to explain all previous data. The (p,p') cross sections for the states in $^{27}$Al show fair agreement in shape, but at both 17.5 and 20.3 MeV they show rather large deviations from the $^{28}$Si $2_1^+$ distribution at angles larger than 80°. The differential cross section for the $7/2^+$ state in the $^{27}$Al (d,d') reaction[17] at 12 MeV was different from that of the other states; Bishop and Lombard[18] have

observed that this state must retain some rotational character to explain their electron scattering results. However, if the discrepancy for the $7/2^+$ asymmetry can be ascribed to a rotational component in its wave function, it is not clear why this does not affect the $9/2^+$ distribution as well.

The strong coupling model has generally been used to describe the levels of the other odd-A nucleus in this investigation, $^{25}Mg$. Asymmetries measured for the low-lying states are shown in Fig. 3. The measured shapes of the differential cross sections at 17.5 MeV for all these states in $^{25}Mg$ are very similar, and the same is true at this energy. The asymmetries, however, show large variations. The 1.61 MeV $7/2^+$ level is the second member of the rotational band built on the ground state; its cross section and asymmetry might thus be expected to closely resemble the corresponding curves for the $2_1^+$ states in $^{24}Mg$ or $^{26}Mg$. This prediction is certainly not precisely fulfilled, although the curves are more similar to the data for $^{24}Mg$ or $^{26}Mg$ than to the data for $^{28}Si$. The 0.58-MeV ($1/2^+$), 0.98-MeV ($3/2^+$), and 1.96-MeV ($5/2^+$) states are the low-lying members of a second rotational band built on a different particle state. The shapes of these asymmetry distributions are not necessarily expected to reflect the shapes of L=2 transitions in the neighboring nuclei or to exactly resemble each other. The variations observed are thus not unreasonable even in terms of the rotational model.

3. <u>The L=4 transitions</u>

Strong transitions to $4^+$ states have been observed at 4.12 and 6.00 MeV in $^{24}Mg$ and at 4.61 MeV in $^{28}Si$; the asymmetry data are illustrated in Fig. 4. Clearly, there is little similarity among the three curves. Differential cross sections for the two states in $^{24}Mg$ are also very different

from each other; the $^{28}$Si cross section is, however, similar in shape to the cross section for the 6.00-MeV state in $^{24}$Mg. As noted above,[16] the differences in the cross sections for the 4.12-MeV state in $^{24}$Mg and the 4.61 MeV state in $^{28}$Si can be explained if $^{28}$Si is assumed to have a large hexadecapole deformation.

4. L=0 transitions

The asymmetries measured for the $0^+$ states at 6.44 MeV in $^{24}$Mg and 3.58 MeV in $^{26}$Mg both show very large amplitude oscillations which are reminiscent of elastic scattering distributions. They are shown in Fig. 5. Cross sections for these states measured at 17.5 MeV were both strongly forward-peaked, but otherwise quite different from each other.

5. Unnatural-parity transitions

Transitions to $3^+$ states were observed in the three even-even nuclei; the asymmetries are illustrated in Fig. 6. Clearly, there is no characteristic shape. The relative cross sections for all these states are rather flat at both 17.5 and 20.3 MeV; there is some structure but it is not the same at the two energies.

6. $^{12}$C, $^{16}$O, and $^{40}$Ca

The asymmetries for the ground states and for low-lying excited states in $^{12}$C, $^{16}$O, and $^{40}$Ca are shown in Figs. 7-9. The data for $^{12}$C are in only qualitative agreement with the data taken by Craig *et al.*[19] at 20.3 MeV; the discrepancies are probably due to the resonances observed at nearby energies. The present data were repeated many times over the course of several months with consistent results. In addition, the $^{16}$O data were taken at the same time. The elastic data for $^{16}$O agree well with the data of Boschitz *et al.*[20]

at 20.7 MeV. However, Lowe[21] has reported resonance structure in $^{16}O$ elastic scattering at 20.3 MeV; this makes the agreement between the 20.3- and the 20.7-MeV data surprising. The elastic data for $^{40}Ca$ are in good agreement with data taken recently at Berkeley[22] at the same energy.

The curve in Fig. 7 showing the asymmetry for the excited $0^+$ state in $^{12}C$ at 7.65 MeV displays the same very large oscillations observed for $0^+$ asymmetries in $^{24}Mg$ and $^{26}Mg$. The asymmetries for the first $2^+$ states in $^{12}C$ and $^{16}O$ at 4.43 and 6.92 MeV (Figs. 8-9) do not resemble each other or the curves for any L=2 transitions in $^{24}Mg$ - $^{28}Si$. The data for the $3^-$ states in $^{16}O$ and $^{40}Ca$ are also quite different from each other. Note that the $3^-$ curve in $^{40}Ca$ is completely out of phase with the $5^-$ curve. Finally, the asymmetries for the $1^-$ and $2^-$ states in $^{16}O$ are also shown in Fig. 8.

## IV. ANALYSIS

### A. Optical Parameters ($^{24}Mg$ - $^{28}Si$)

The determination of optical parameters for $^{24}Mg$ - $^{28}Si$ is complicated by the strong coupling between the excited states and the ground state. In their analysis of inelastic alpha scattering in the rare-earth region, Hendrie *et al.*[23] obtained excellent results by first obtaining optical-model parameters for a nearby spherical nucleus, and then using these same parameters in coupled-channels calculations for the deformed nuclei. Unfortunately there is no nearby spherical nucleus to use as a starting point for the present analysis. In addition, it is not clear that the "spherical" parameters should remain constant, since the mass of these nuclei is low. The addition of spin also

makes the parameter search more difficult. Finally, since we neglect possible spin-spin forces in the optical potential and the angular-dependent terms in the full Thomas form of the spin-orbit term in the optical potential, the parameters for odd-A nuclei might be expected to be somewhat different from the parameters for even-A nuclei.

The search code MERCY, a modified version of SEEK,[24] was used to obtain simultaneous fits to the elastic cross sections and polarizations; the coupling to the excited states was neglected. The definition of the optical potential and the search procedures employed are standard;[1] the absolute normalization of the data was included in the search. Errors on the cross sections were uniformly set at ± 10%; the errors on the polarization were fixed at ± 0.03. Corrections arising from the finite angular acceptance of the detectors were not included.

Calculations were carried out with three different sets of fixed geometrical parameters which have appeared in the literature.[25] The strength parameters $V$, $W_D$, and $V_{so}$, and the spin-orbit radius $r_{so}$ were left as free parameters in the searches. The values of $\chi^2/N$ ranged from 9.0 for $^{25}Mg$ to 28.5 for $^{28}Si$.

Since the fixed-geometry searches did not yield very good fits to the data, a search on all nine parameters of the optical potential was performed. This search produced the fits to the elastic polarizations and cross sections shown in Figs. 10-11. These fits are still only fair, especially in comparison with the fits found in Ref. 1 for $^{90}Zr$, $^{92}Zr$, and $^{92}Mo$. The final parameter values are listed in Table II. The nucleus to nucleus variations are considerable, much larger than the variations in the parameters for the heavy

nuclei. Some of these variations could be considerably reduced with little sacrifice in the quality of the fit. It is interesting to note that $r_{so}$ is generally at least 20% smaller than the central radius; in heavier nuclei this difference is usually about 10 - 15%.

Since it has sometimes been found necessary[4] to have very good fits to the elastic polarization in order to obtain good fits to inelastic asymmetry data, searches were also made on the polarization data alone for $^{24}$Mg and $^{28}$Si. However, the best fits are very little better than those illustrated in Fig. 11. Better fits were obtained by including an imaginary spin-orbit term with a strength between 0.0 and + 1.0 MeV. However, the inclusion of this term makes the $2^+$ asymmetry predictions considerably worse.

## B. Coupled Channels and DWBA

The Oxford coupled-channels program[26] was used to interpret the inelastic scattering cross sections and asymmetries. Both rotational and vibrational models are allowed; the entire optical potential can be deformed. In the vibrational model, terms up to second order in the Taylor expansion of the optical potential can be included. In the rotational model, on the other hand, the calculation is correct to all orders in the interaction potential, since a Legendre expansion is used. In the small coupling limit, where the DWBA is valid, the two models give the same results. When the coupling is sufficiently strong, however, the predictions need not be similar, and cross section and asymmetry measurements can in principle distinguish between the models. However, the predictions for the vibrational model may be sensitive to the number of terms retained in the Taylor expansion.

Both the vibrational and rotational models assume that the nuclear surface should be represented by the shape:

$$R(\theta,\phi) = R_o[1 + \Phi(\theta,\phi)]$$

where

$$\Phi(\theta,\phi) = \sum_{\lambda\mu} \alpha_{\lambda\mu} Y_\lambda^\mu(\theta,\phi) \quad ;$$

$\alpha_{\lambda\mu}$ is directly related to the deformation parameter $\beta_\lambda$ and $Y_\lambda^\mu$ is a spherical harmonic. In the rotational model, $\beta$ represents the static deformation of the nucleus in the rotational band built upon the ground state. In the vibrational model, $\beta$ is a dynamical deformation parameter which describes the amplitude of the vibrations about a spherical equilibrium state. The form that the optical potential $U(r)$ takes under this deformation is not well-defined.[6] Two methods have generally been used. The first is to replace $U(r)$ by $U(r-R)$. The second is to replace $R_o$, whenever it appears in the undeformed potential, by $R(\theta)$. The two methods give equivalent descriptions of the inelastic scattering provided the deformation of the spin-orbit term in the potential is not important. The two methods do not, however, yield equivalent forms of the deformed spin orbit term (DSO). The first method yields the form used in previous vibrational-model calculations by the Saclay group.[1] It will be referred to as type I:

$$V_{so}(r) = \frac{R_o}{a^2 r^2} 2e(1+e)^{-3}[a(1+e) + r(e-1)] \quad , \qquad (2)$$

where e is $\exp[r-R_o A^{1/3}/a]$. The second method has been used by the Oak Ridge group[4] and others, and yields the form which will be referred to as type II:

$$V_{so}(r) = \frac{R_o}{a^2 r^2} 2e(1+e)^{-3} [r(e-1)] \quad . \tag{3}$$

Note that type I includes an extra term inside the brackets.

In addition to these two methods, the full Thomas (FT) form of the deformed spin-orbit potential has also been used with success by Sherif and Blair.[7] They write the spin-orbit term in the optical potential as follows:

$$U_s(r,\theta,\phi) = \left(\frac{\hbar}{m_\pi c}\right)^2 \sigma \cdot [\nabla \rho(r) \times \frac{\nabla}{i}] \quad , \tag{4}$$

where $\rho(r)$ is the nuclear matter density. If the angular dependence of the gradient operator acting on $\rho(r)$ is neglected, this expression reduces to the standard $\ell \cdot \sigma$ form. The angle-dependent terms can affect the inelastic predictions, and generally they have been found[7] to improve the fits to inelastic asymmetry and spin-flip data. The Oxford program does not include the full Thomas form, but some DWBA calculations have been carried out with the program of Sherif and the results are described below. The radial part of the FT deformed spin-orbit potential in his program is equivalent to the type II term above.

Coupled-channels calculations with type I and type II terms have been performed for the $0^+$, $2_1^+$, and $4_1^+$ states in $^{24}Mg$ and $^{28}Si$. Our primary interest, of course, lies in the quality of the predictions of the $2_1^+$ and $4_1^+$ asymmetries. However, we also want to know whether the asymmetry data can distinguish between rotational and vibrational models, and between positive and negative deformations. The CC calculations shown here used optical parameters which were not adjusted from the spherical values; only the fine details of the asymmetry predictions are affected when the adjusted values are used.

1. Elastic scattering and polarization

When the parameters of Table II are used in a CC calculation, the predicted elastic scattering polarization and cross section are changed considerably. This comparison is illustrated in Figs. 12-13 for $^{24}Mg$. A deformation parameter $\beta_2$ of 0.49 was assumed for the rotational and vibrational model calculations and coupling to the first $2^+$ and $4^+$ states was included. The curves labeled DWBA are the spherical optical-model fits to the data; they are identical to those shown in Figs. 10-11. The quality of the fit to the elastic polarization data between 60-90° is improved when the strong coupling is included; at back angles, however, the CC fit is somewhat worse. For the cross section, the DWBA fit is considerably better than the other two.

If the spherical optical model parameters are adjusted by decreasing $V_o$ and $W_D$, the CC fit to the cross section can be made almost as good as the spherical fit. When this is done, the CC polarization prediction is almost identical to the spherical prediction at angles up to 100°. To improve the CC polarization fit at back angles requires finer parameter adjustments.

Further calculations show that the predictions of both the elastic polarization and the cross section are little affected by the inclusion of the $4_1^+$ state unless some $\beta_4$ deformation is added. The predictions do depend, of course, on whether the entire optical potential is deformed, or just certain parts of it. For the curves of Figs. 12-13, all terms, real, imaginary, and spin-orbit, were deformed. The predictions of the elastic scattering are not sensitive to the type of spin-orbit deformation.

2. <u>The $2^+$ states</u>

Predictions of the asymmetry and cross sections for the $2_1^+$ state in $^{24}$Mg and $^{28}$Si are shown in Figs. 14-15. All curves illustrated have been calculated with the entire optical potential deformed, since the predictions of the asymmetry are almost invariably improved by the inclusion of deformed imaginary and spin-orbit terms. The DSO term has little effect on the cross sections; the effect of complex coupling on the cross-section predictions is variable. In the CC calculations shown, the ground-state, the $2_1^+$ state, and the $4_1^+$ state have generally been included. When no direct transition to the $4_1^+$ state was allowed, i.e., when $\beta_4$ was set to zero, the $4_1^+$ state could be omitted from the CC calculation with almost no effect on the $0^+$ and $2^+$ predictions.

The value of $\beta_2$ for $^{24}$Mg was set to +0.49, the value obtained in a CC analysis of 49.5-MeV inelastic proton scattering by Rush and Ganguly.[11] Since absolute cross sections were not obtained in the present work, this value could not be checked. However, a very similar value, +0.47, has been

recently obtained from the CC analysis of 17.5-MeV proton scattering.[16] For $^{28}$Si, the value of $\beta_2$ was generally set at 0.55, the value obtained in several DWBA analyses of proton scattering.[9,27] However, the CC analysis of the 17.5 MeV data[16] gives a $\beta_2$ of about 0.34. Thus, the effects of the strong coupling are somewhat overestimated for $^{28}$Si. When a non-zero value of $\beta_4$ was included in the present calculations, it was set to +0.33. The values of $\beta_4$ obtained from the 17.5 MeV analysis[16] are -0.05 for $^{24}$Mg and +0.25 for $^{28}$Si.

The CC rotational-model prediction for the $2_1^+$ asymmetry in $^{24}$Mg is shown in Fig. 14A; a type II DSO term was used with the optical parameters of Table II. It is clear that the forward maximum is not predicted, whereas the back-angle peak is fitted fairly well. If the parameters are adjusted to fit the elastic cross-section, almost no change is observed in the predicted asymmetry of the $2_1^+$ state. The forward maximum appears also in data at higher energies,[4,11] at smaller angles; the high-energy fits are also poor at this maximum, unless the magnitude of the DSO term is arbitrarily increased.

Curves 1 and 2 in Fig. 14B correspond to DWBA calculations with a type II DSO term, with and without the angle-dependent term of the full-Thomas spin-orbit potential. The CC rotational model calculation (curve 3) is the curve of Fig. 14A. Note that the effect of including the strong coupling in the calculation is to reduce the predicted maximum near 70°, while including the FT term increases it (curve 2).

Illustrated in Fig. 14C are three curves with a type I DSO term. The DWBA prediction (curve 1) is positive at the 70° maximum, and is quite similar to the FT curve (2) in Fig. 14B. The radial part of the FT deformed spin-orbit

term is of type II. The fact that curve 1 is similar to the FT prediction indicates that the FT prediction could be improved by including a type I radial part instead of type II. The other two curves in Fig. 14B are CC vibrational-model calculations with the expansion extended to first and second order, respectively. Including the first-order coupling (curve 2) decreases the 70° maximum considerably; the second-order term increases it again, but shifts it out of phase (curve 3). Since the difference between curves 2 and 3 is so large, it is reasonable to assume that some of the differences between the rotational-model calculations (Fig. 14A) and these vibrational-model calculations may be due to the neglect of third and higher order terms in the vibrational expansion.

Some CC predictions for $^{28}$Si asymmetries are shown in Fig. 15. The three curves correspond to rotational-model calculations (type II) with $\beta_2 = +0.55$ (1), and $\beta_2 = -0.55$ (2), and a second-order vibrational model calculation (type I) with $\beta_2 = 0.55$ and $\beta_4 = 0.33$. Since the recent measurement of the quadrupole moment of the $2_1^+$ state indicates that $^{28}$Si has an oblate deformation,[14] we should expect the rotational model prediction with a negative $\beta_2$ to give the best agreement. In fact, the oblate prediction is better than the prolate prediction, but both are far from reproducing the forward maximum. It is interesting, however, that the measured asymmetry for $^{28}$Si at the 70° maximum is more positive than for $^{24}$Mg; at least this difference is predicted by the calculations. However, both rotational-model predictions are worse than the vibrational-model curve, although the neglect of third and higher order terms may be important, as discussed above. Note finally that for a given type of calculation the asymmetry predictions for $^{24}$Mg and $^{28}$Si

are very similar, even though the optical parameters of Table II are quite different.

The fits to the cross sections shown in Figs. 16-17 are fair. Rotational model CC curves are shown, $\beta_2$ is positive for $^{24}Mg$ and negative for $^{28}Si$. The parameters of Table II are used. The main effect of adjusting these parameters to fit the elastic scattering is to change the absolute magnitude of the predictions, but the normalization here is arbitrary. However, the modifications also tend to improve the fits at back angles. Many other cross section predictions have been made, with different values of $\beta$, with different optical parameters, and with the vibrational model. Generally the differences between these predicted angular distributions are too small to be experimentally distinguishable.

3. <u>The $4^+$ states</u>

The $4^+$ state of a rotational band built upon a $0^+$ ground state cannot be excited in first order unless the nucleus has a hexadecapole deformation. A two-phonon state in a vibrational model must also be excited by a multiple-excitation process, whereas a one-phonon vibrational state can be excited in first order. Predictions of the asymmetry for the $4_1^+$ states in $^{24}Mg$ and $^{28}Si$ for these modes of excitation are shown in Figs. 18-19. Type I DSO terms were used in the vibrational-model calculations, and type II DSO terms were used in the rotational-model calculations. Agreement with the experimental data is uniformly poor.

Illustrated in Fig. 18A is the CC rotational-model curve for $^{24}Mg$ with $\beta_2$ only ($\beta_4$ was found to be very small in the work of Ref. 16). Again, the prediction is not sensitive to the optical parameters.

The predictions of other model assumptions are shown in Fig. 18B. Curve (1) is the same type of calculation as shown in Fig. 18A, but $\beta_4$ deformation has been included. Curve (2) is a CC vibrational-model calculation for a two-phonon $4^+$ state, with $\beta_2$ only. Curve (3) is a CC vibrational-model calculation for a one phonon $4^+$ state; both $\beta_2$ and $\beta_4$ are included. The differences between the predicted curves are quite large, but none gives any hint of a large peak at about 60°. The two-phonon prediction (curve 2) is reasonably similar to the curve of Fig. 18A; neither includes first-order contributions. The two curves (1 and 3) which do include first-order contributions are similar at forward angles.

The rotational-model prediction for $^{28}$Si is shown in Fig. 19A; $\beta_2$ and $\beta_4$ are included. The inclusion of $\beta_4$ was necessary to account for the shape and magnitude of the 17.5 MeV cross section, but it does not improve the fit to the asymmetry. In Fig. 19B are two DWBA curves, the one with a type I DSO term, and the other with the FT term. The two are very similar and fail to reproduce the data.

The fits obtained to the $4_1^+$ cross sections for $^{24}$Mg and $^{28}$Si are presented in Figs. 20-21. The CC rotational-model curve for $^{24}$Mg with $\beta_2$ only (Fig. 20) does not give a good fit with the parameters of Table II; readjusting the parameters to fit the elastic scattering improves the agreement at back angles. The CC rotational model prediction for $^{28}$Si (Fig. 21) includes $\beta_4$ and gives a reasonably good fit to the data. Without $\beta_4$, the prediction is very similar to the prediction for $^{24}$Mg. Vibrational-model calculations for the $4^+$ states closely resemble the rotational-model calculations. The rotational-model curve calculated without $\beta_4$ resembles a two-phonon

vibrational-model curve; with $\beta_4$, the rotational-model prediction is similar to a one-phonon vibrational-model prediction.

4. $^{40}$Ca

Both macroscopic and microscopic calculations have been carried out for the first $3^-$ and $5^-$ states in $^{40}$Ca. The microscopic curves have been calculated by R. Schaeffer[28] using the wave functions of Gillet and Sanderson.[29] The cross sections and asymmetries that he has computed are shown in Figs. 22-23. The contribution of the knock-on exchange amplitudes has been included to a good approximation in some of these curves; a Serber exchange mixture was assumed. The effects of exchange on the absolute magnitude of the predicted cross sections are large and clearly important; however, the shapes of the asymmetries and differential cross sections are not grossly changed. The asymmetry for the $5_1^-$ state shows reasonable agreement, either with or without exchange, but the cross section does not; for the $3_1^-$ state, the cross section prediction is reasonably good, but the asymmetry is poorly fit.

The DWBA macroscopic-model predictions of the asymmetry are illustrated in Fig. 24. The fits are somewhat better than the fits obtained with the microscopic model. The full Thomas term improves the fit to the asymmetry of the $5_1^-$ state but makes the agreement for the $3_1^-$ state somewhat worse. The good agreement with the $5_1^-$ state is interesting because it indicates that the difficulties with the $4_1^+$ states in $^{24}$Mg and $^{28}$Si do not arise simply because of the high spin of these states.

## V. SUMMARY AND DISCUSSION

Asymmetries measured for a given value of the angular momentum transfer show rather large differences from one nucleus to the neighboring one, although some gross features of the curves remain constant, such as the peaks at 70° and 120° for L=2 transitions. The differential cross sections for a given L transfer also vary widely. The shapes, however, generally agree quite well with those measured by Crawley and Garvey[9] at 17.5 MeV. In addition, the forward peak in the L=2 asymmetries has also been observed at 30, 40, and 49 MeV. These two observations indicate that compound nucleus contributions are not important, except perhaps for excited $0^+$ states and unnatural parity states which have small cross sections. Some discrepancies with the predictions of a pure weak-coupling model for $^{27}$Al were found, especially in the shapes of the asymmetries for the $5/2^+$ and $7/2^+$ levels at 2.73 and 2.21 MeV. Very large asymmetries were measured for excited $0^+$ states, comparable in magnitude to the polarization in elastic scattering. The shapes of the asymmetry curves for 3+ states showed the largest nucleus-to-nucleus variations.

The theoretical analysis of the $2_1^+$ and $4_1^+$ asymmetries in $^{24}$Mg and $^{28}$Si yielded disappointing results. These results must be considered preliminary in the sense that no search was made on the optical parameters with the effects of strong coupling included. However it is unlikely that a set of optical parameters can be found to reproduce the $2^+$ and $4^+$ asymmetries. We have in fact tried a large number of parameter sets without success; the predictions are not very sensitive to the parameters. Further, the one adjustment of the optical parameters which does make a significant improvement in the fits to the elastic polarization, viz., the inclusion of a positive imaginary spin-orbit potential, makes the fits to the asymmetries considerably worse.

The effects of strong coupling are important in describing both the elastic and inelastic asymmetries and cross sections. Differences were usually found between the predictions of the rotational and vibrational models, but neither gave a good fit to the data for L=2 or L=4 transitions. Some of the differences between the two models may be due to the neglect of terms of higher than second order in the vibrational model expansion. The predicted asymmetries for $^{28}$Si with a positive and a negative deformation parameter are also significantly different, but both are in poor agreement with the data. The analysis of the $4_1^+$ asymmetries in $^{24}$Mg and $^{28}$Si adds no new information on the hexadecapole deformations of these nuclei.

Calculations were performed with two different types of radial dependence in the deformed spin-orbit term, and also with the full Thomas expression of the spin-orbit term. The type I predictions (Eq. (2)) were consistently better than the type II predictions (Eq. (3)) for L=2 transitions. Differences between these two types of calculation have previously been found to be very small for heavier nuclei. The FT predictions are also superior to the type II curves; a comparison of a rotational model CC curve with an FT (DWBA) prediction reveals a clear preference for the latter. However, the FT (DWBA) and type I (DWBA) predictions can hardly be distinguished from each other.

Microscopic- and macroscopic-model DWBA predictions of the asymmetries of the $3_1^-$ and $5_1^-$ states in $^{40}$Ca yielded fair agreement with the experimental data. The vibrational model fit to the $5^-$ asymmetry is quite good, in fact, when the full Thomas term is included. Thus the failure to obtain good fits to the $4^+$ states in $^{24}$Mg and $^{28}$Si cannot be ascribed simply to the high spin.

## ACKNOWLEDGMENTS

The authors are grateful for the indispensable help of the technical staff at the Saclay cyclotron; we want to thank in particular R. Chaminade, A. Garin, R. Manse and H. Poussard. We are indebted also to A. D. Hill for his coupled-channels program and to W. S. Hall for his peak-stripping program. The visitors to Saclay greatly appreciate the hospitality of the Center. Two of us (A.G.B. and R.deS.) wish to acknowledge the financial support of NATO during part of this work.

## REFERENCES


1. C. Glashausser, R. de Swiniarski, J. Thirion, and A. D. Hill, Phys. Rev. 164, 1437 (1967).
2. C. Glashausser, R. de Swiniarski, J. Goudergues, R. M. Lombard, B. Mayer, and J. Thirion, to be published in Phys. Rev.
3. D. J. Baugh, M. J. Kenny, J. Lowe, D. L. Watson, and H. Wojciechowski, Nucl. Phys. A99, 203 (1967).
4. M. P. Fricke, E. E. Gross, and A. Zucker, Phys. Rev. 163, 1113 (1967).
5. V. E. Lewis, E. J. Burge, A. A. Rush, and D. A. Smith, Nucl. Phys. A101, 589 (1967).
6. Cf. C. Glashausser and J. Thirion, Advances in Nuclear Physics, Vol. II, M. Baranger and E. Vogt, editors, (Plenum Press, New York, 1968), p. 79.
7. H. Sherif and J. Blair, Phys. Letters 26B, 489 (1968); H. Sherif, thesis, Univ. of Washington, 1968, (unpublished), and Nucl. Phys. A131, 532 (1963).
8. A. Blair, P. A. Vaganov, C. Glashausser, J. Goudergues, R. M. Lombard, B. Mayer, R. de Swiniarski, and J. Thirion, Akademia Nauk SSSR Izvestia, Seria Fizicheskaia, 32, 814 (1968); English translation: Columbia Technical Translations, 32, 750 (1969).
9. G. M. Crawley and G. T. Garvey, Phys. Rev. 160, 981 (1967).
10. R. Beurtey and J. M. Durand, Nucl. Instr. Methods 57, 313 (1967).
11. A. A. Rush and N. K. Ganguly, Nucl. Phys. A117, 101 (1968).
12. J. Kokame, I. Nonaka, M. Koike, K. Matsuda, H. Kamitsubo, Y. Awaya, T. Wada, and H. Nakamura, Proceedings of the International Conference on Nuclear Structure, Tokyo, 1967, p. 351.

13. G. Ripka, Advances in Nuclear Physics, I, M. Baranger and E. Vogt, editors, (Plenum Press, New York, 1968).

14. T. K. Alexander, D. Pelte, O. Häusser, B. Hooton, and H. C. Evans, Bull. Am. Phys. Soc. 14, 555 (1969).

15. J. Bar-Touv and A. Goswami, Phys. Letters 28B, 391 (1969).

16. R. de Swiniarski, C. Glashausser, D. L. Hendrie, J. Sherman, A. D. Bacher, and E. A. McClatchie, Phys. Rev. Letters 23 No. 6, 317 (1969).

17. H. Niewodniczański, J. Nurzyński, A. Stralkowski, J. Wilczynski, J. R. Rook, and P. E. Hodgson, Nucl. Phys. 55, 386 (1964).

18. R. M. Lombard and G. R. Bishop, Nucl. Phys. A101, 601 (1967).

19. R. M. Craig, J. C. Dore, G. W. Greenlees, J. Lowe, and D. L. Watson, Nucl. Phys. 79, 177 (1966).

20. E. T. Boschitz, M. Chabre, H. E. Conzett, and R. J. Slobodrian, Proceedings of the Second International Symposium on Polarization Phenomena of Nucleons, Karlsruhe, 1965, P. Huber and H. Schopper, editors (Birkhauser Verlag, Basel, 1966), p. 331.

21. J. Lowe, private communication.

22. R. de Swiniarski, A. D. Bacher, J. Ernst, A. Luccio, F. Resmini, R. Slobodrian, and W. Tivol, Bull. Am. Phys. Soc. 13, 1663 (1968).

23. D. L. Hendrie, N. K. Glendenning, B. G. Harvey, O. N. Jarvis, H. H. Duhm, J. Saudinos, and J. Mahoney, Phys. Letters 26B, 127 (1968).

24. M. A. Melkanoff, J. Raynal, and T. Sawada, UCLA Report No. 66-10, January, 1966 (unpublished).

25. G. R. Satchler, Nucl. Phys. A92, 273 (1967); F. G. Perey, Phys. Rev. 131, 745 (1963); P. Kossanyi-Demay and R. de Swiniarski, Nucl. Phys. A108, 577 (1968).

26. A. D. Hill, unpublished notes.

27. R. W. Barnard and G. D. Jones, Nucl. Phys. A108, 655 (1968).

28. R. Schaefer, private communication.

29. V. Gillet, A. Green, and E. Sanderson, Nucl. Phys. 88, 321 (1966); V. Gillet and E. Sanderson, Nucl. Phys. 91, 292 (1967).

Table I.

| Target | Thickness ($mg/cm^2$) | Purity (%) |
|---|---|---|
| Mylar | 1.0 | -- |
| $^{24}Mg$ | 1.0 | 99.5 |
| $^{25}Mg$ | 1.7 | 99.5 |
| $^{26}Mg$ | 2.3 | 99.8 |
| $^{27}Al$ | 1.4 | natural |
| $^{28}Si$ | 3.7 | natural |
| $^{40}Ca$ | 1.0 | natural |

Table II.

| | $V$ (MeV) | $W_D$ (MeV) | $V_{so}$ (MeV) | $r_o$ (f) | $a_o$ (f) | $r_I$ (f) | $a_I$ (f) | $r_{so}$ (f) | $a_{so}$ (f) | $\chi^2_\sigma$ | $\chi^2_p$ | $\chi^2/N$ | $\sigma_R$ (mb) |
|---|---|---|---|---|---|---|---|---|---|---|---|---|---|
| $^{24}Mg$ | 47.8 | 8.46 | 5.15 | 1.21 | 0.61 | 1.14 | 0.54 | 0.97 | 0.32 | 37 | 301 | 8.68 | 711 |
| $^{25}Mg$ | 42.82 | 6.88 | 4.18 | 1.26 | 0.67 | 1.42 | 0.37 | 1.04 | 0.34 | 80 | 178 | 6.32 | 665 |
| $^{26}Mg$ | 55.43 | 9.68 | 9.00 | 1.15 | 0.67 | 1.31 | 0.42 | 0.80 | 0.97 | 117 | 137 | 5.34 | 744 |
| $^{27}Al$ | 51.34 | 10.08 | 7.14 | 1.17 | 0.67 | 1.37 | 0.34 | 0.90 | 0.80 | 112 | 172 | 6.93 | 712 |
| $^{28}Si$ | 45.57 | 7.91 | 4.08 | 1.20 | 0.65 | 1.44 | 0.41 | 0.97 | 0.35 | 76 | 185 | 7.31 | 760 |

FIGURE CAPTIONS

Fig. 1. Measured values of the asymmetry normalized to 100% beam polarization for L=2 transitions in $^{24}Mg$, $^{26}Mg$, and $^{28}Si$. The curves are visual guides.

Fig. 2. Measured asymmetries for transitions in $^{27}Al$. The curves are visual guides.

Fig. 3. Measured asymmetries for transitions in $^{25}Mg$. The curves are visual guides.

Fig. 4. Measured asymmetries for L=4 transitions in $^{24}Mg$ and $^{28}Si$. The curves are visual guides.

Fig. 5. Measured asymmetries for L=0 transitions in $^{24}Mg$ and $^{26}Mg$. The curves are visual guides.

Fig. 6. Measured asymmetries for $3^+$ states. The curves are visual guides.

Fig. 7. Measured polarization in elastic scattering from $^{12}C$, $^{16}O$, and $^{40}Ca$. The asymmetry for the excited $0^+$ state at 7.65 MeV in $^{12}C$ is also shown. The curves are visual guides.

Fig. 8. Measured asymmetries for transitions in $^{16}O$. The curves are visual guides.

Fig. 9. Measured asymmetries for several transitions in $^{12}C$ and $^{40}Ca$. The curves are visual guides.

Fig. 10. Optical-model predictions of the elastic scattering cross sections. The parameters are those of Table II; no coupling was included.

Fig. 11. Optical-model predictions of elastic scattering polarization. The parameters are those of Table II; no coupling was included.

Fig. 12. Coupled-channels calculations of the elastic scattering polarization. The rotational and first-order vibrational model curves assume a $\beta_2$ of

0.49. The curve labeled DWBA was calculated with a $\beta_2$ of 0.01 with the coupled-channels program.

Fig. 13. Coupled-channels calculations of the elastic scattering cross sections. The deformation parameters are the same as for Fig. 12.

Fig. 14. (A) CC rotational-model prediction, type II DSO, $\beta_2 = 0.49$. (B) 1) DWBA prediction, type II DSO. 2) DWBA prediction, full Thomas spin-orbit term. 3) CC rotational-model prediction, type II DSO, $\beta_2 = 0.49$. (C) 1) DWBA prediction, type I DSO. 2) CC vibrational-model prediction, first order, type I DSO, $\beta_2 = 0.49$. 3) CC vibrational-model prediction, second-order, type I DSO, $\beta_2 = 0.49$.

Fig. 15. Predictions of the asymmetry for the 1.77-MeV $2^+$ state in $^{28}$Si. 1) CC rotational-model prediction, type II DSO, $\beta_2 = 0.55$. 2) Same as 1) but $\beta_2 = -0.55$. 3) CC vibrational-model predictions, second order, type I DSO, $\beta_2 = 0.55$, $\beta_4 = 0.33$.

Fig. 16. Predicted cross section for the $2_1^+$ state of $^{24}$Mg; the CC rotational-model was used with $\beta_2 = 0.49$.

Fig. 17. Predicted cross section for the $2_1^+$ state of $^{28}$Si; the CC rotational-model was used with $\beta_2 = -0.55$, $\beta_4 = 0.33$.

Fig. 18. Predicted asymmetries for the $4_1^+$ state of $^{24}$Mg. (A) CC rotational-model prediction, type II DSO, $\beta_2 = 0.49$. (B) 1) CC rotational-model prediction, type II DSO, $\beta_2 = 0.49$, $\beta_4 = 0.30$. 2) CC vibrational-model calculation, type I DSO, one-phonon state, $\beta_2 = 0.49$, $\beta_4 = 0.30$. 3) CC vibrational-model calculation, type I DSO, two-phonon state, $\beta_2 = 0.49$.

Fig. 19. Predicted asymmetries for the $4_1^+$ state of $^{28}Si$. (A) CC rotational-model prediction, type II DSO, $\beta_2 = -0.55$, $\beta_4 = 0.33$. (B) 1) DWBA prediction, type I DSO term. 2) DWBA prediction, full Thomas spin-orbit term.

Fig. 20. Predicted cross section for the $4_1^+$ state in $^{24}Mg$; the CC rotational model was used with $\beta_2 = 0.49$.

Fig. 21. Predicted cross section for the $4_1^+$ state in $^{28}Si$; the CC rotational model was used with $\beta_2 = -0.55$, $\beta_4 = 0.33$.

Fig. 22. Microscopic-model predictions of the asymmetry and cross section for the $3_1^-$ state in $^{40}Ca$, calculated by R. Schaeffer.

Fig. 23. Microscopic-model predictions of the asymmetry and cross section for the $5^-$ state in $^{40}Ca$, calculated by R. Schaeffer.

Fig. 24. DWBA predictions of the asymmetries for the $3_1^-$ and $5_1^-$ states in $^{40}Ca$ with FT and type I DSO terms.

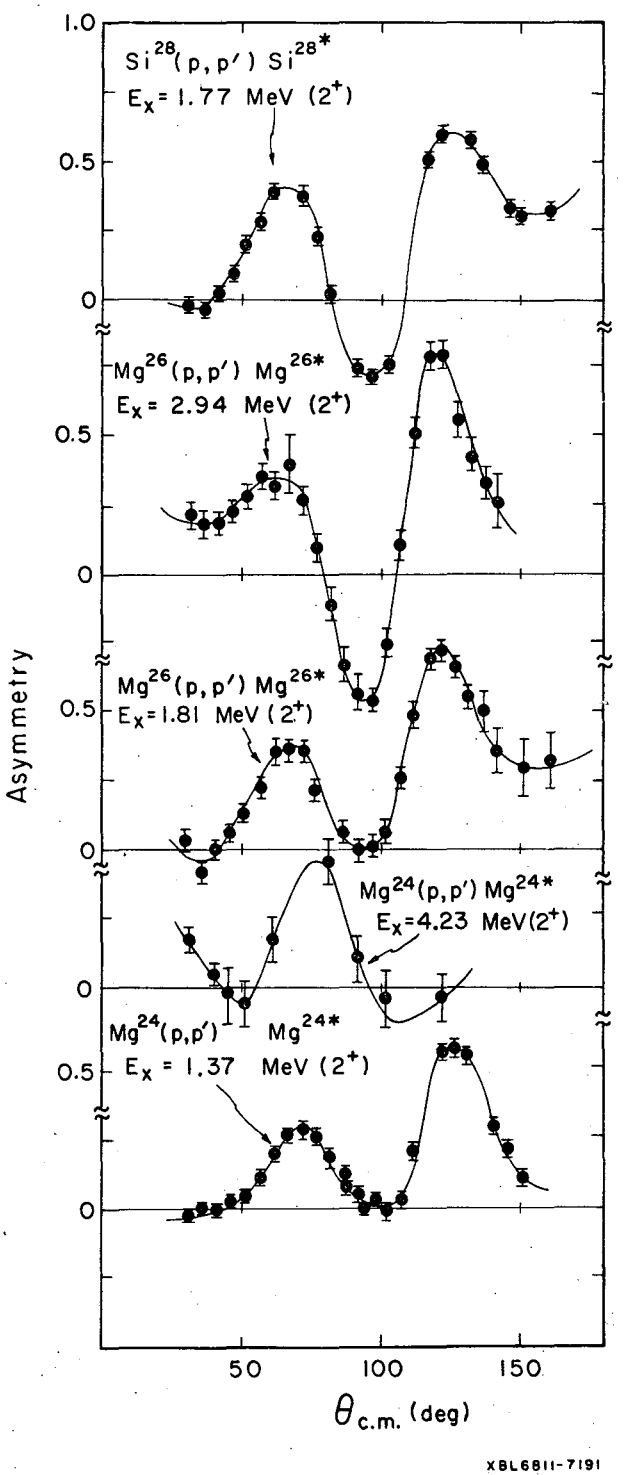
1.0
0.5
0
Si28(p,p′) Si28*
Ex= 1.77 MeV (2+)
Mg26(p,p′) Mg26*
Ex= 2.94 MeV (2+)
Mg26(p,p′) Mg26*
Ex=1.81 MeV (2+)
Mg24(p,p′) Mg24*
Ex=4.23 MeV(2+)
Mg24(p,p′) Mg24*
Ex = 1.37 MeV (2+)
Asymmetry
50
100
150
θc.m. (deg)
XBL6811-7191

Fig. 1

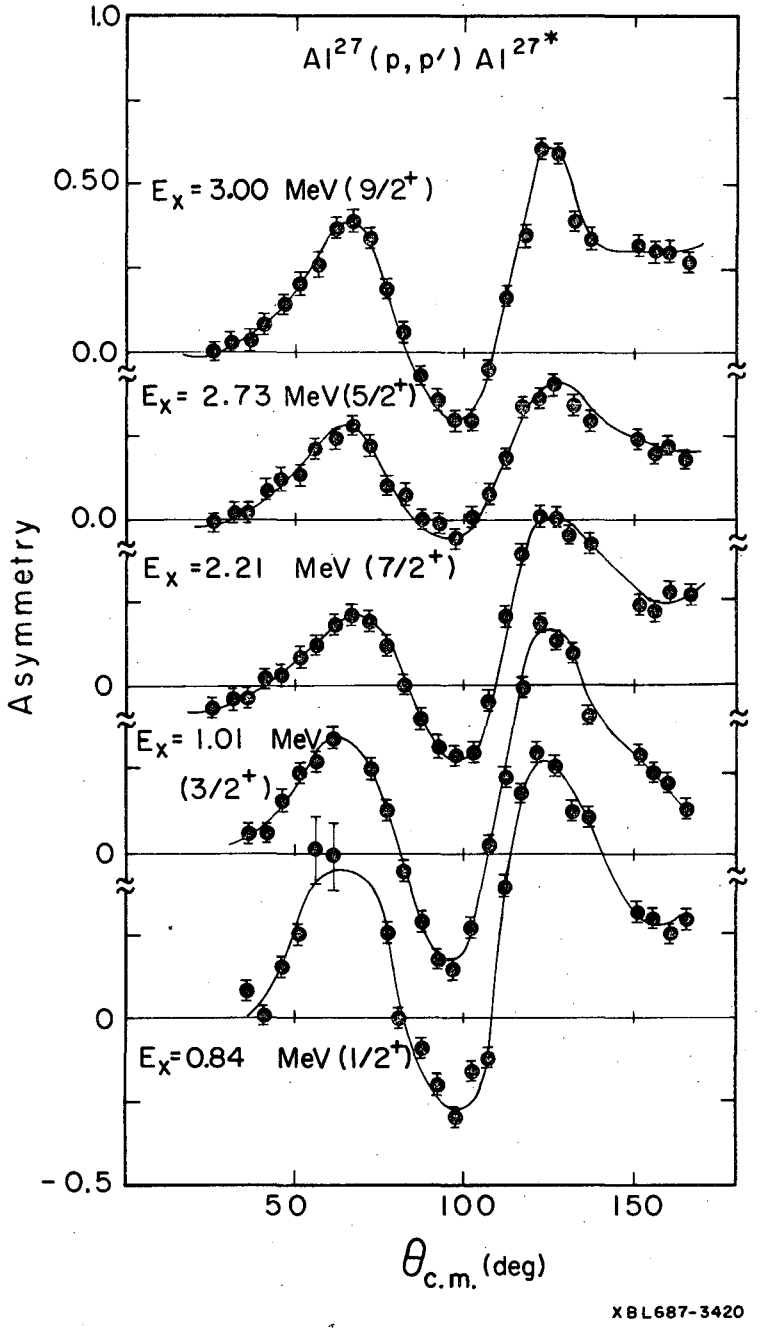
Al27 (p, p′) Al27*
Ex = 3.00 MeV (9/2+)
Ex = 2.73 MeV (5/2+)
Ex = 2.21 MeV (7/2+)
Ex = 1.01 MeV (3/2+)
Ex = 0.84 MeV (1/2+)
Asymmetry
1.0
0.50
0.0
0.0
0
0
0
-0.5
50
100
150
θc.m. (deg)
XBL687-3420

Fig. 2

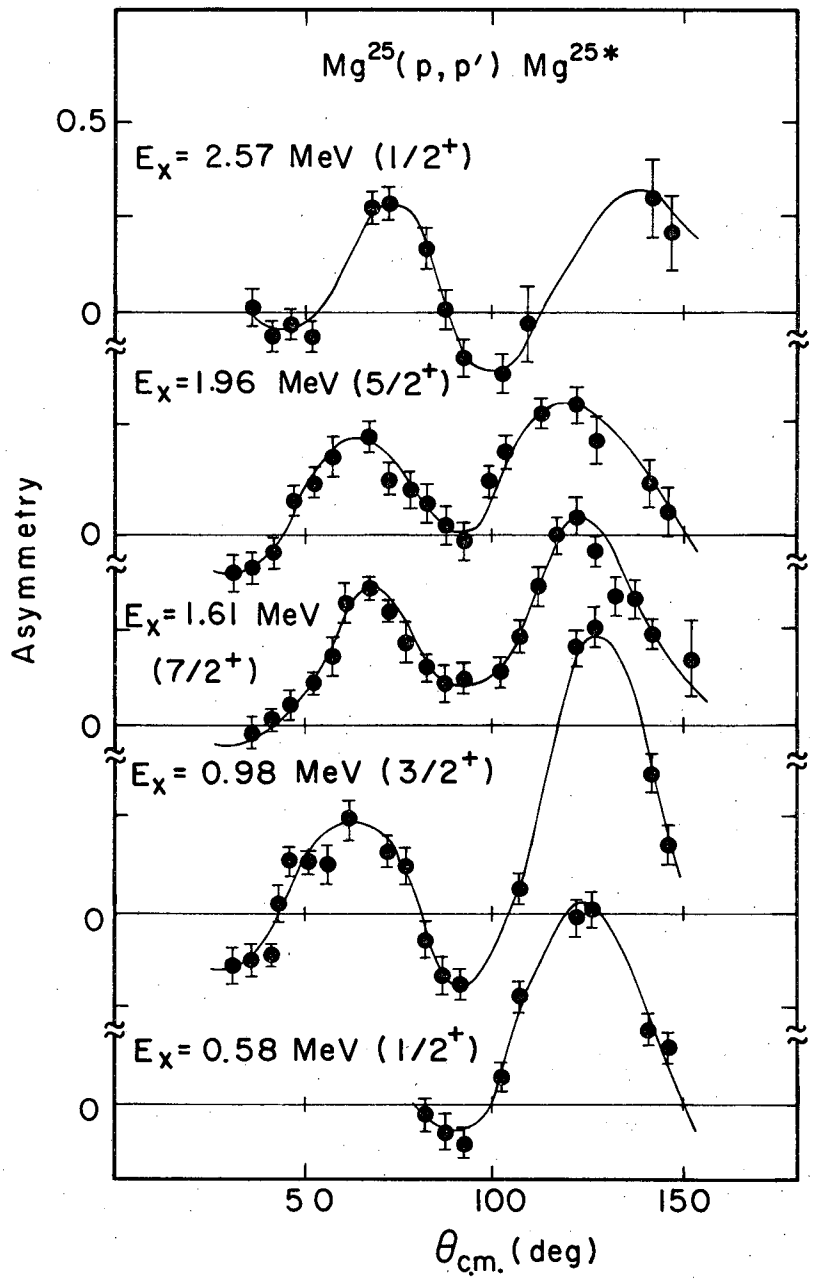


XBL687-3412

Fig. 3

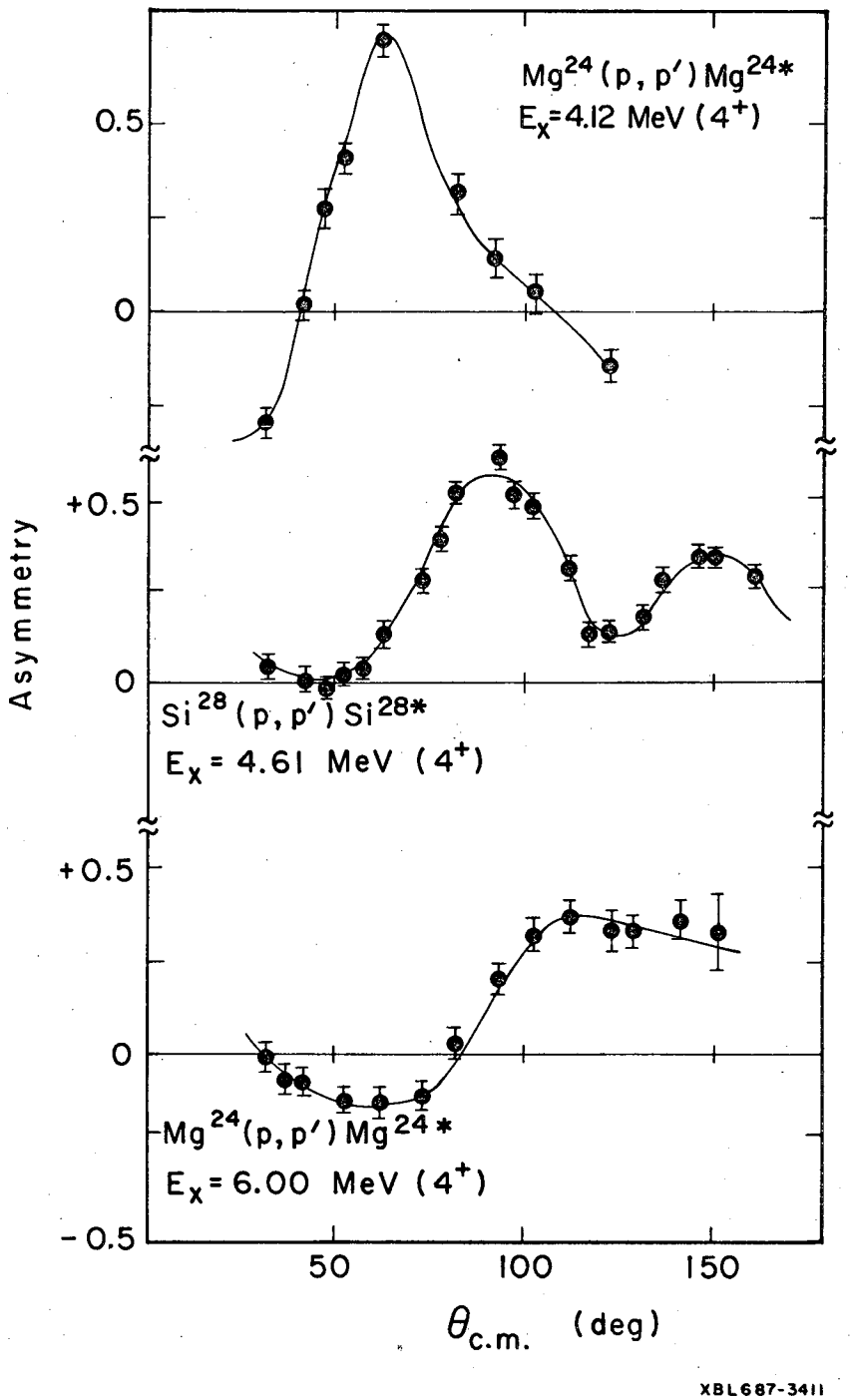
Mg24 (p, p′) Mg24*
Ex=4.12 MeV (4+)
0.5
0
+0.5
0
Si28 (p, p′) Si28*
Ex = 4.61 MeV (4+)
+0.5
0
Mg24(p, p′) Mg24*
Ex = 6.00 MeV (4+)
-0.5
Asymmetry
50
100
150
θc.m. (deg)
XBL687-3411

Fig. 4

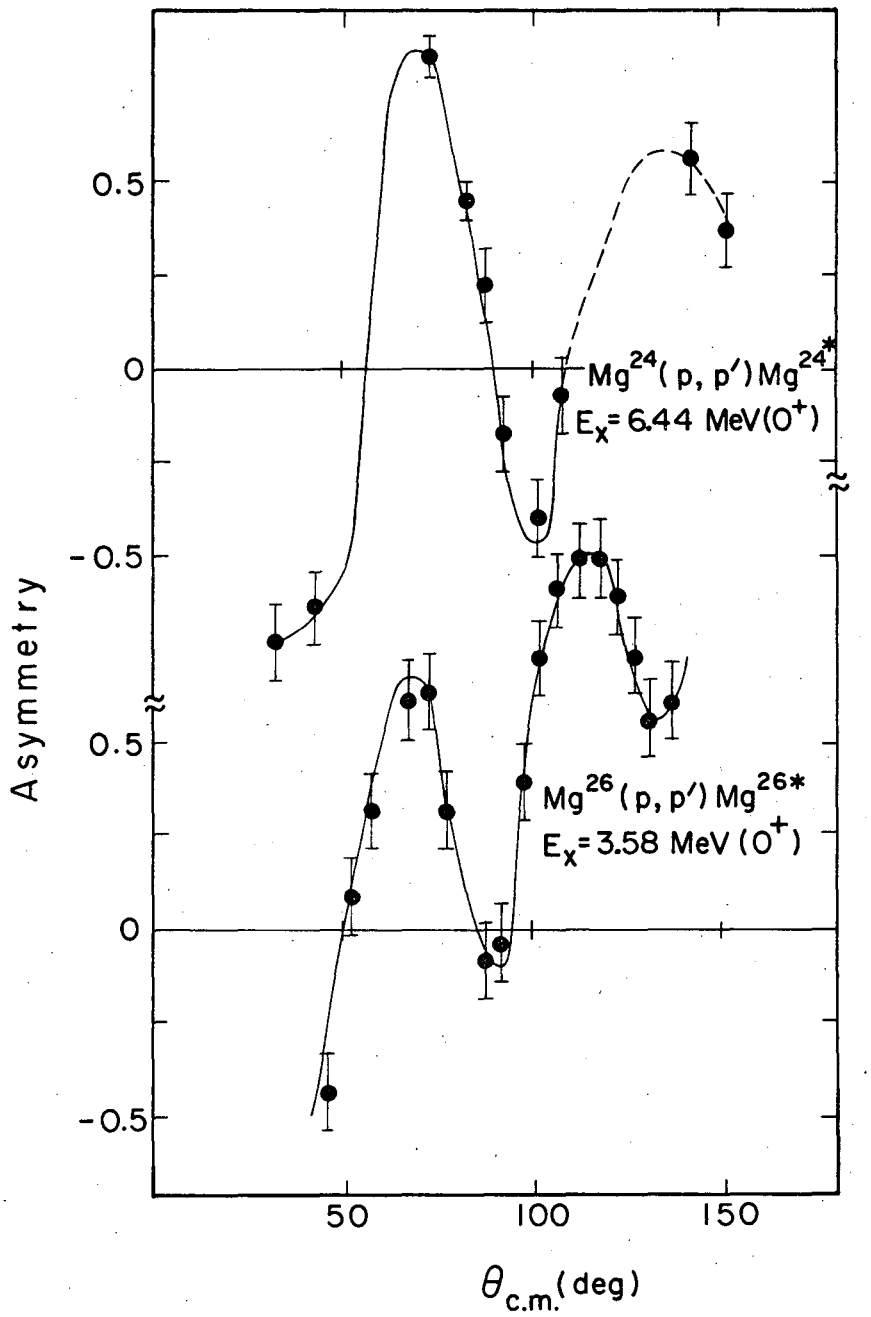


XBL6811-7188

Fig. 5

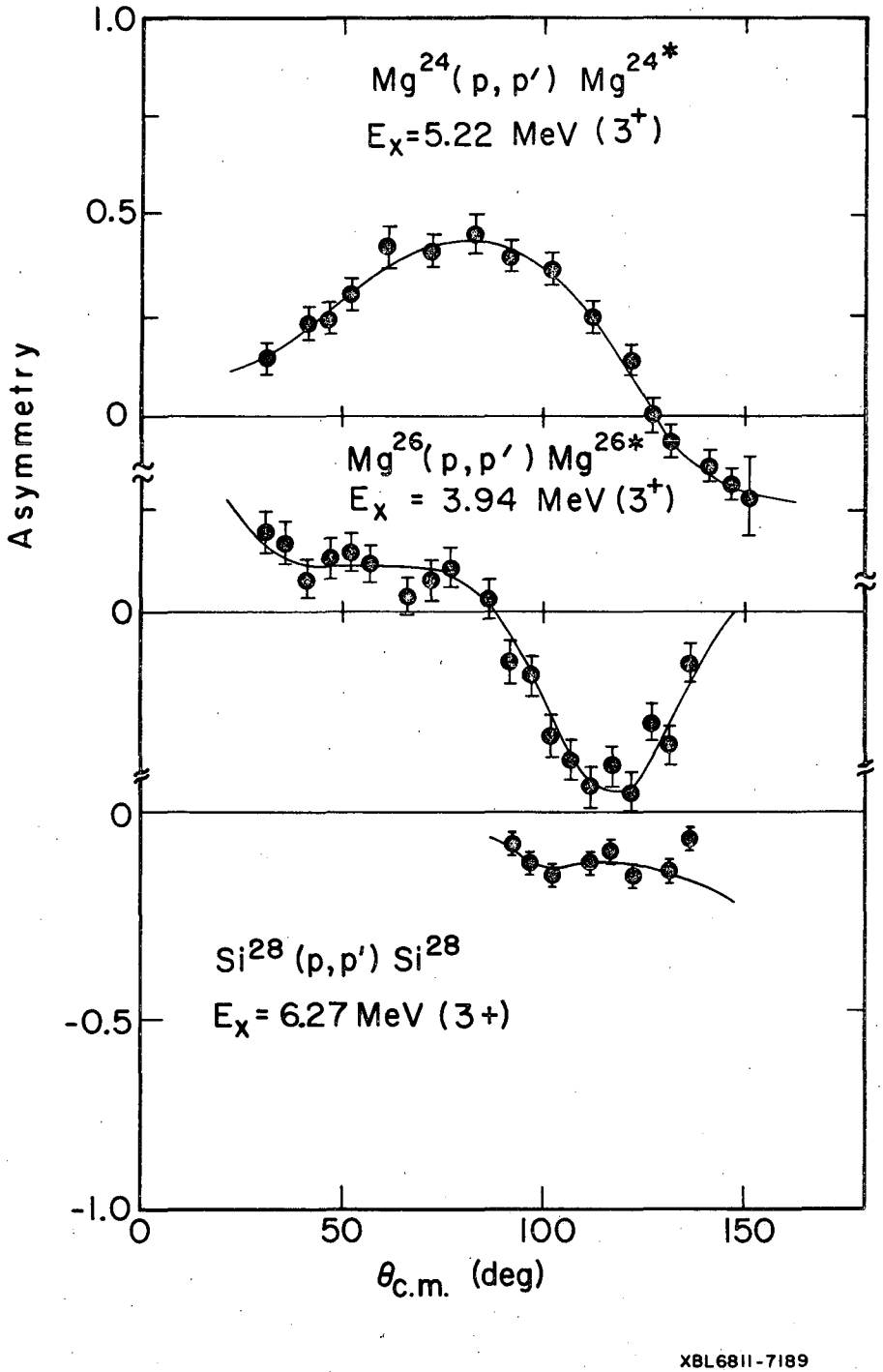
1.0
0.5
0
0
0
-0.5
-1.0
Asymmetry
Mg24(p, p′) Mg24*
Ex=5.22 MeV (3+)
Mg26(p,p′) Mg26*
Ex = 3.94 MeV (3+)
Si28 (p,p′) Si28
Ex= 6.27 MeV (3+)
0
50
100
150
θc.m. (deg)
XBL6811-7189

Fig. 6

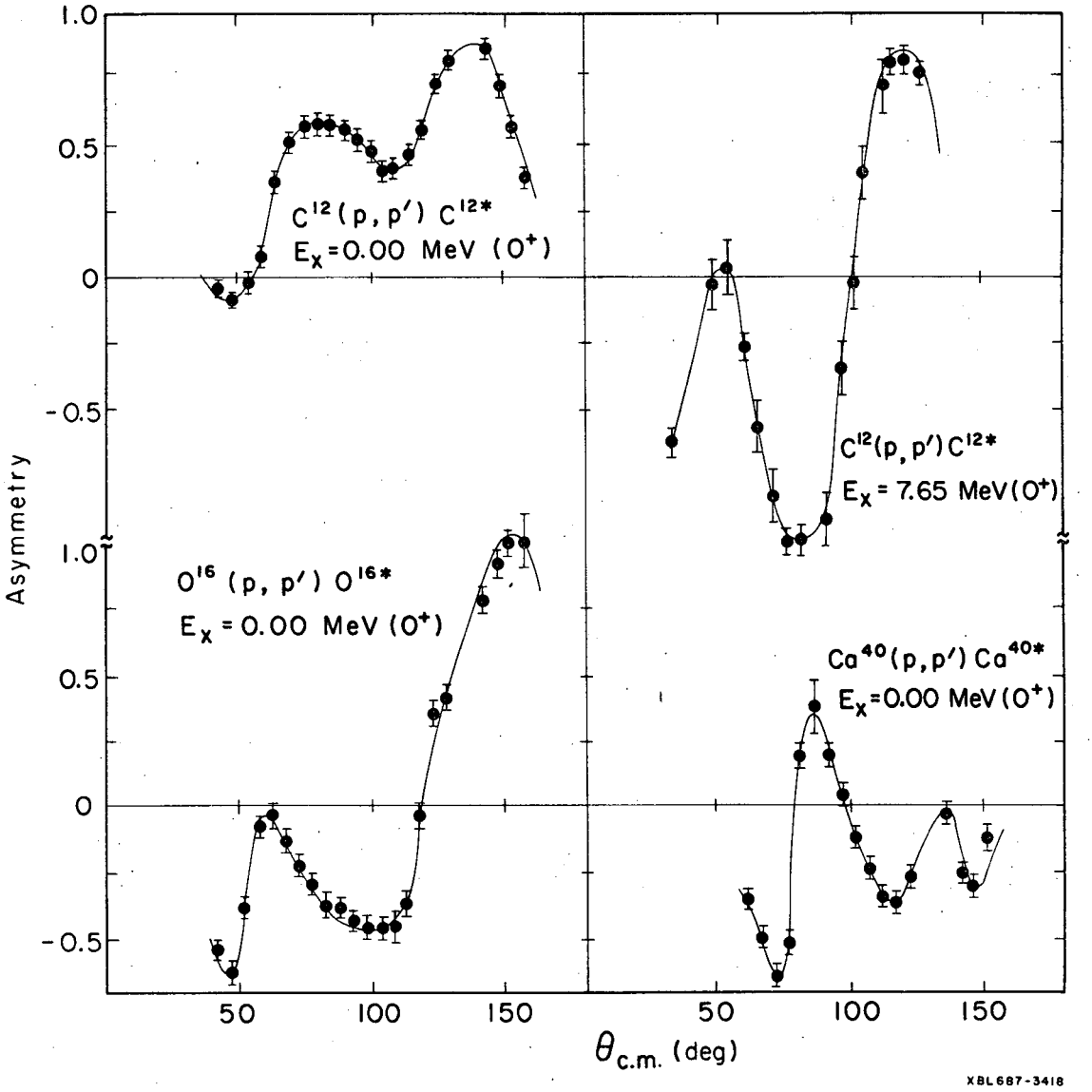
1.0
0.5
0
-0.5
Asymmetry
$C^{12}(p,p')C^{12*}$
$E_x$=0.00 MeV ($0^+$)
$C^{12}(p,p')C^{12*}$
$E_x$ = 7.65 MeV($0^+$)
$O^{16}(p,p')O^{16*}$
$E_x$ = 0.00 MeV ($0^+$)
$Ca^{40}(p,p')Ca^{40*}$
$E_x$=0.00 MeV($0^+$)
50
100
150
$\theta_{c.m.}$ (deg)
XBL687-3418

Fig. 7

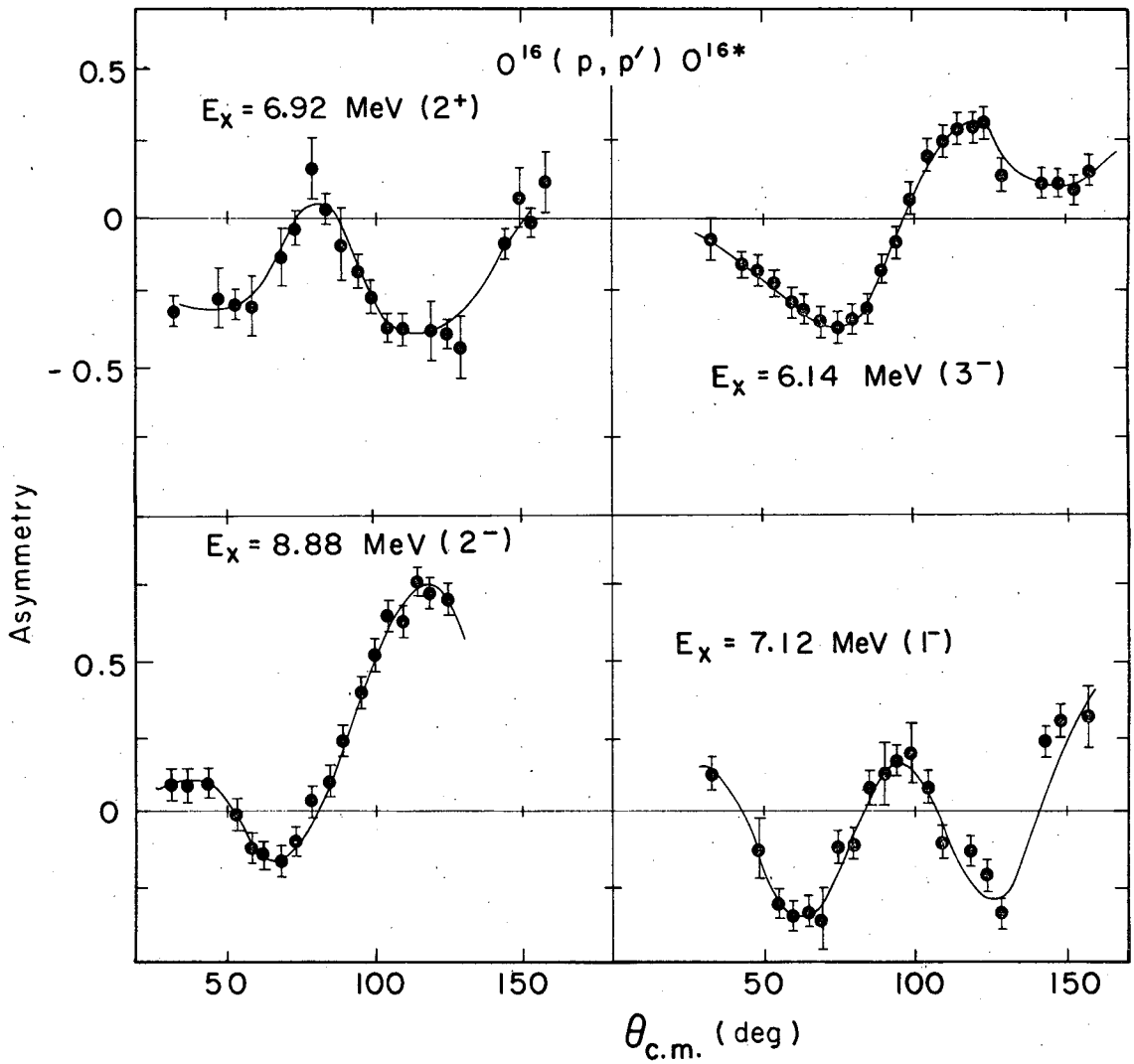
O16 ( p, p′ ) O16*
Ex = 6.92 MeV (2+)
Ex = 6.14 MeV (3−)
Ex = 8.88 MeV (2−)
Ex = 7.12 MeV (1−)
Asymmetry
0.5
0
- 0.5
0.5
0
50
100
150
50
100
150
θc.m. ( deg )
XBL687-3417

Fig. 8

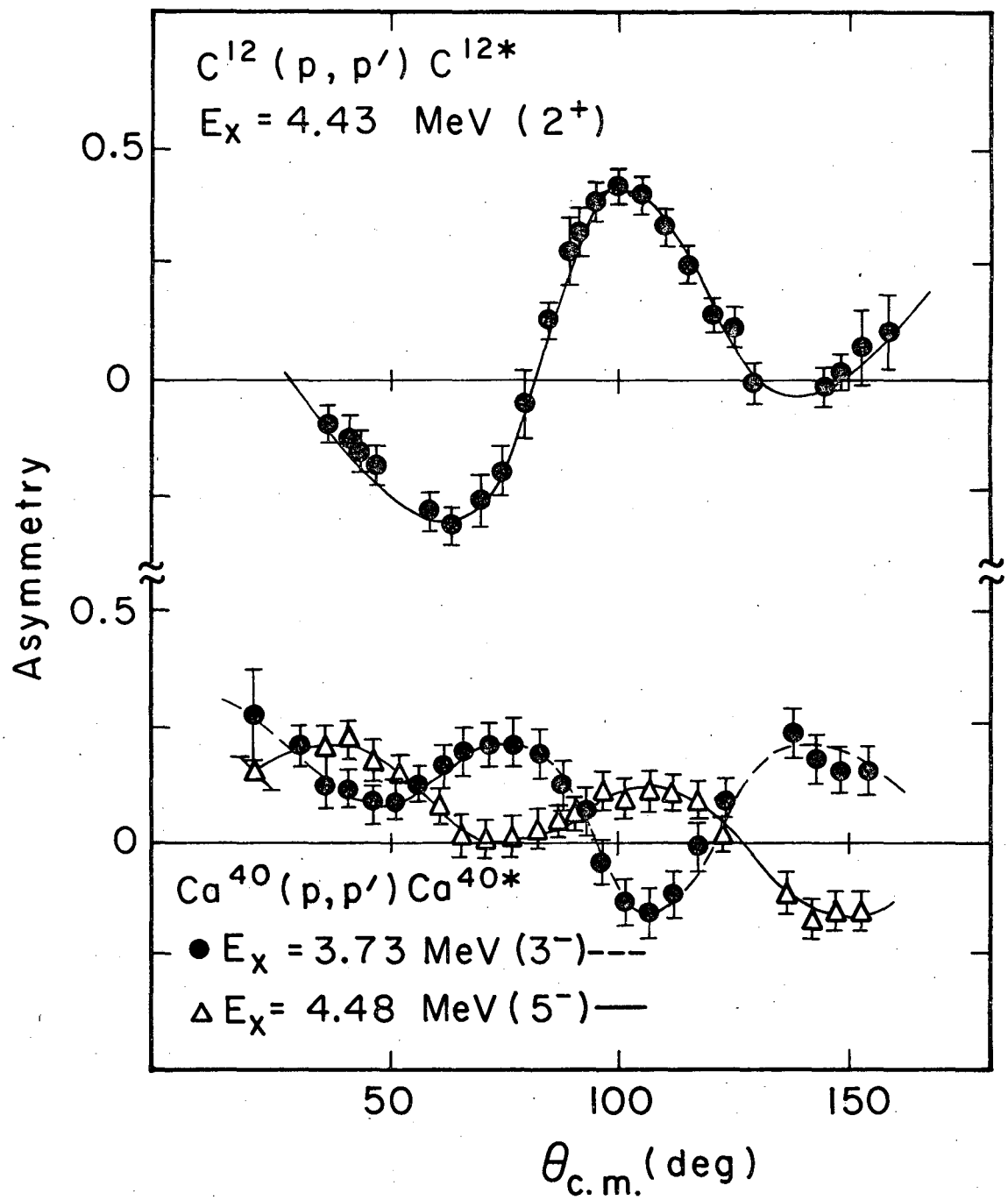


XBL687-3415

Fig. 9

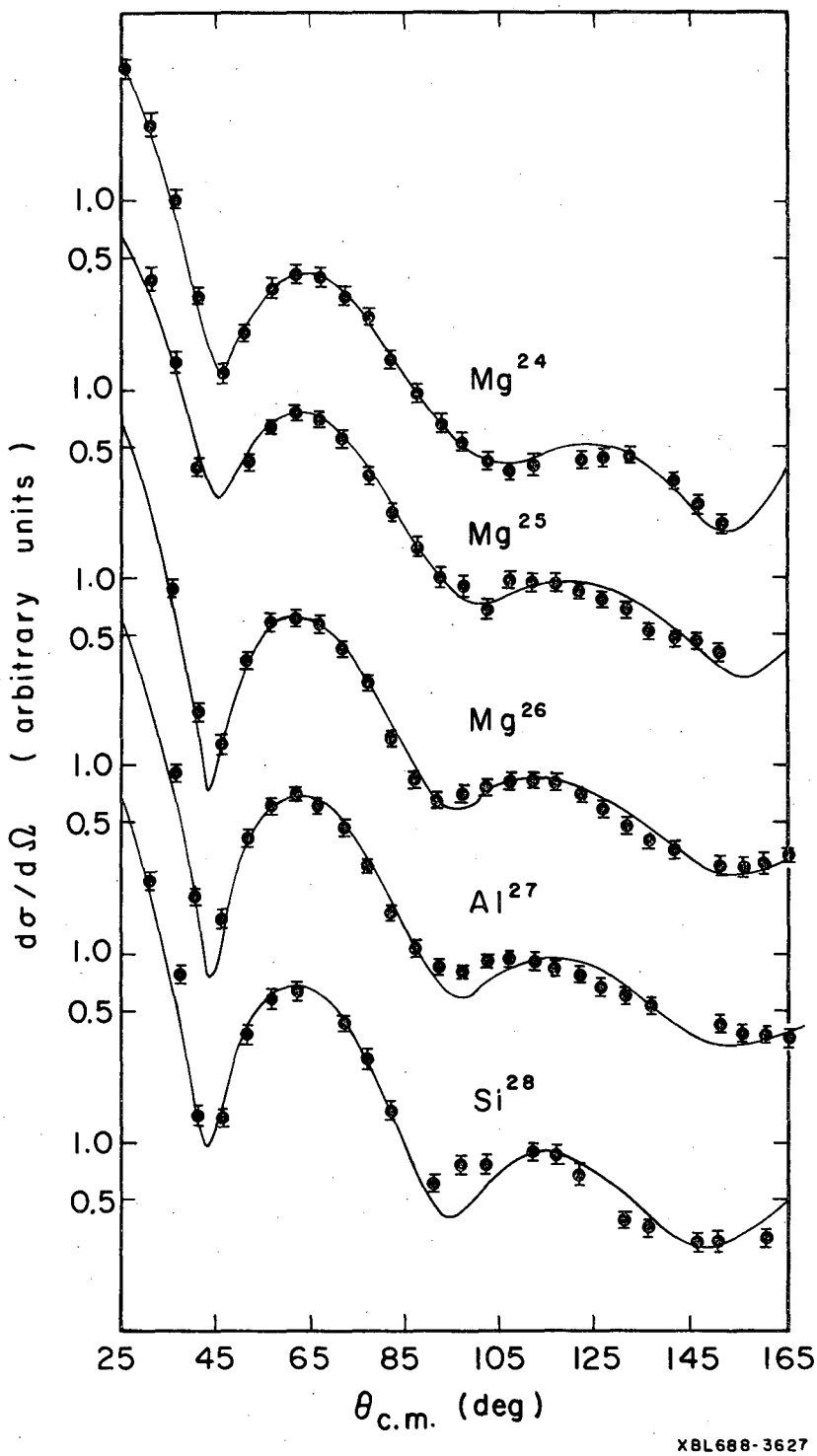
1.0
0.5
Mg24
Mg25
Mg26
Al27
Si28
dσ/dΩ (arbitrary units)
25
45
65
85
105
125
145
165
θc.m. (deg)
XBL688-3627

Fig. 10

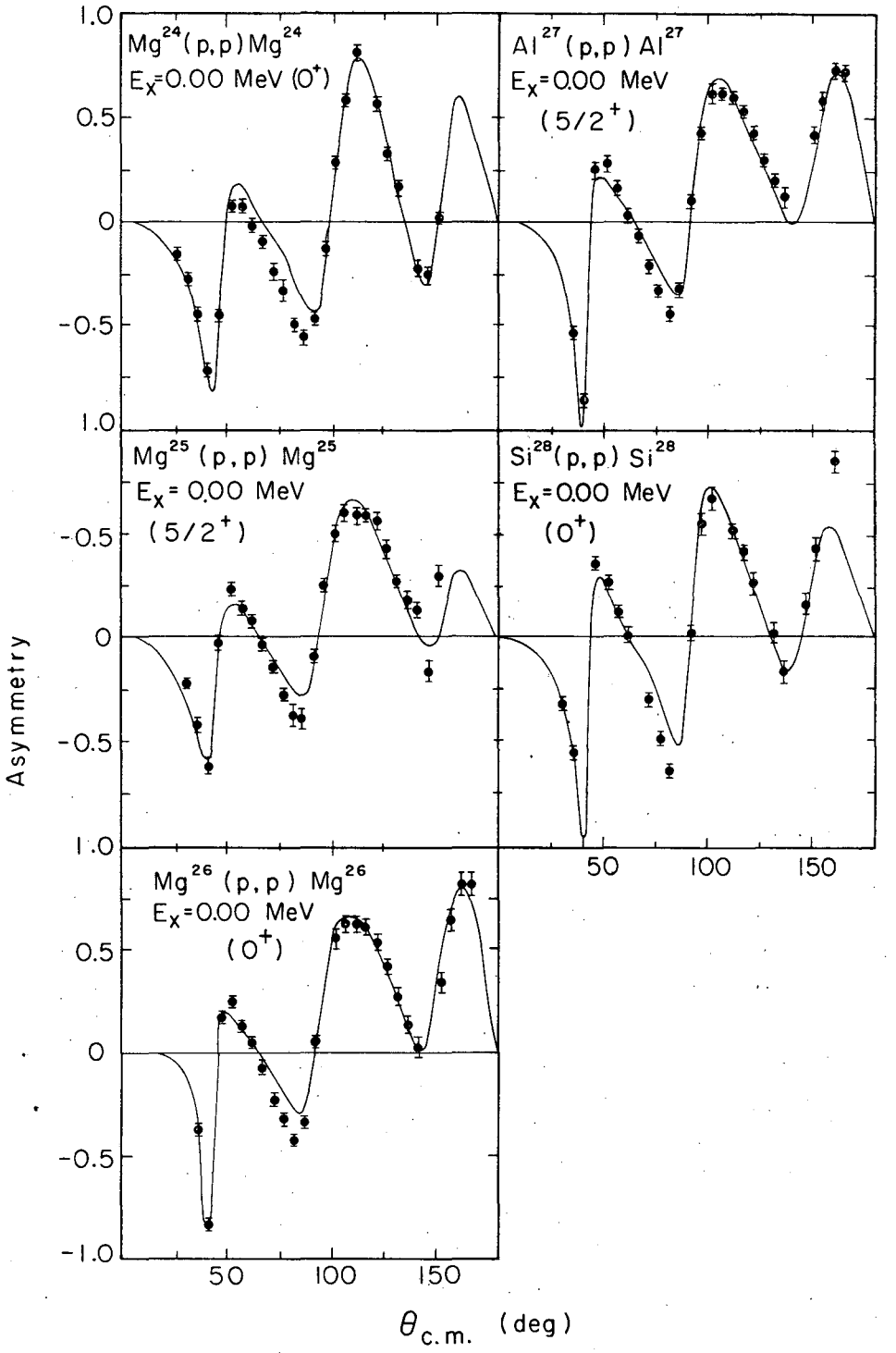


XBL 668-3634

Fig. 11

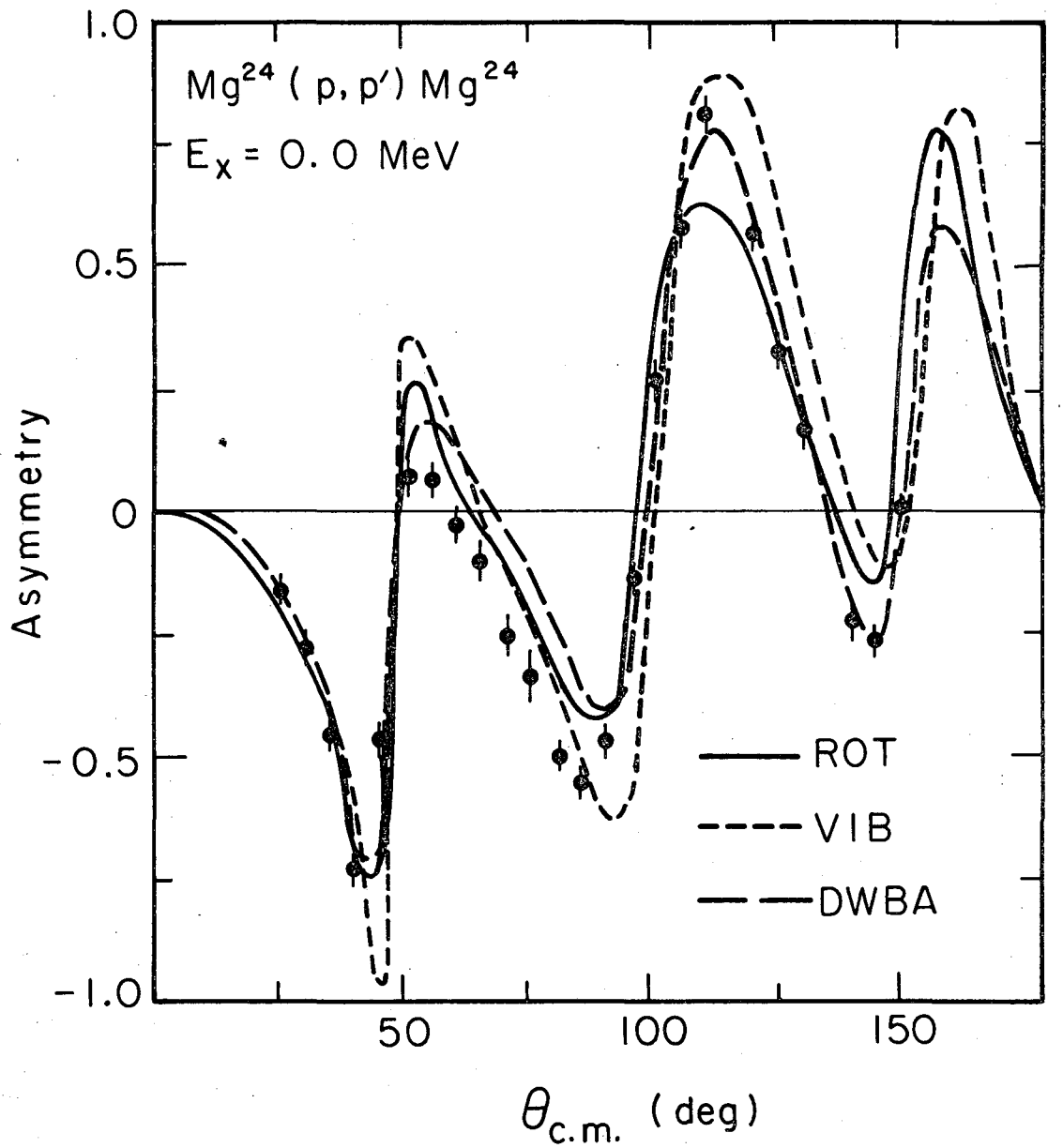


XBL695-2881

Fig. 12

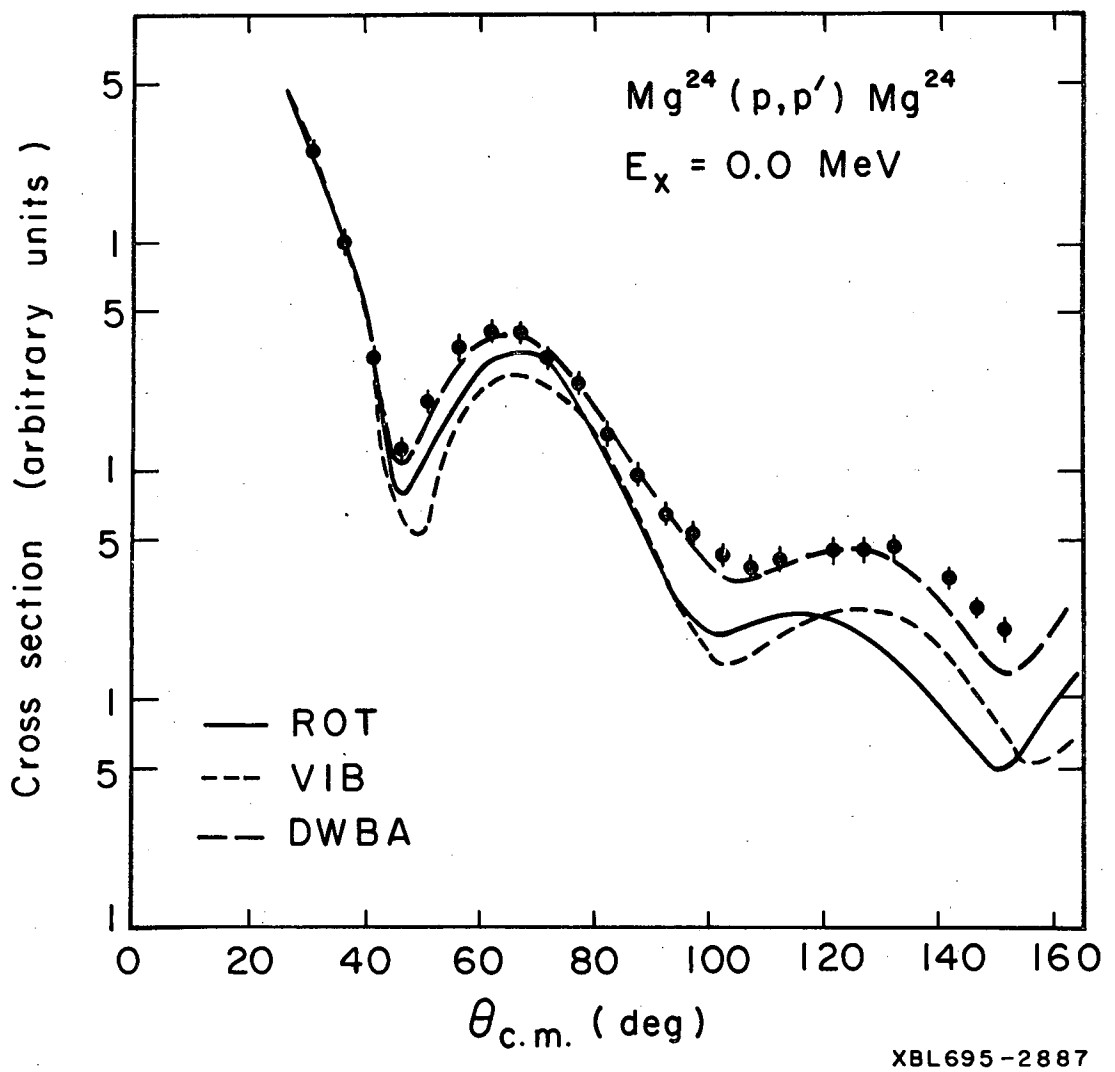
Mg24 (p,p′) Mg24
Ex = 0.0 MeV
ROT
VIB
DWBA
Cross section (arbitrary units)
θc.m. (deg)
5
1
5
1
5
1
5
1
0
20
40
60
80
100
120
140
160
XBL695-2887

Fig. 13

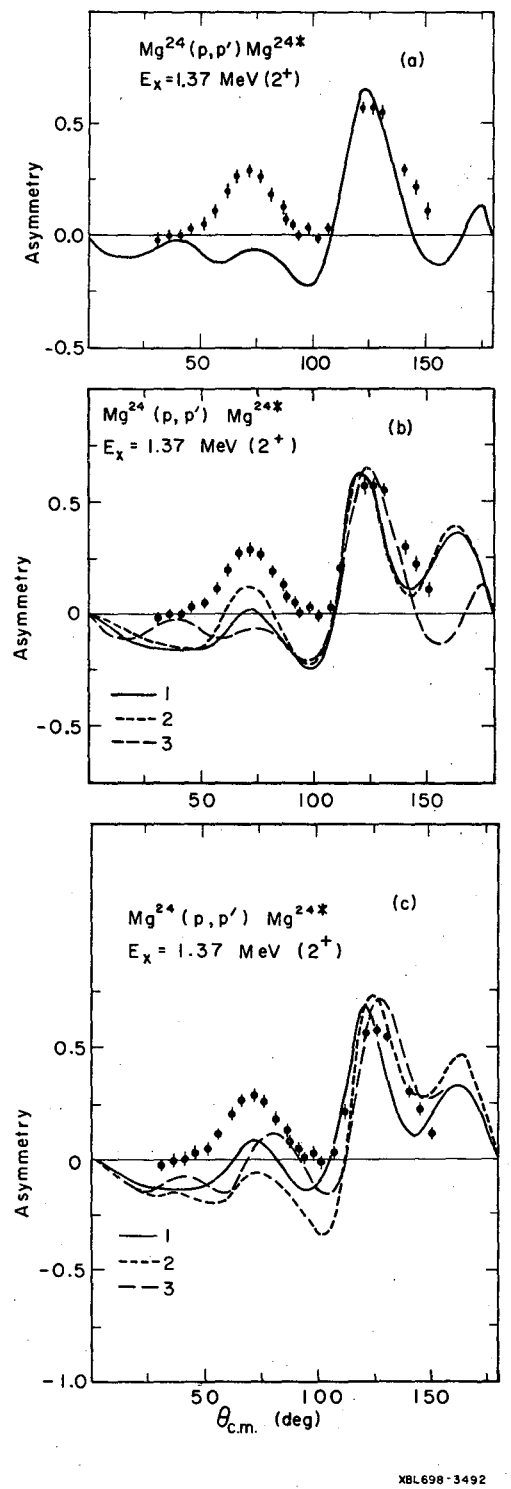
Mg24 (p,p') Mg24*
Ex=1.37 MeV (2+)
(a)
Asymmetry
0.5
0.0
-0.5
50
100
150
Mg24 (p, p') Mg24*
Ex = 1.37 MeV (2+)
(b)
Asymmetry
0.5
0
-0.5
1
2
3
50
100
150
Mg24 (p,p') Mg24*
Ex = 1.37 MeV (2+)
(c)
Asymmetry
0.5
0
-0.5
-1.0
1
2
3
50
100
150
θc.m. (deg)
XBL698-3492

Fig. 14

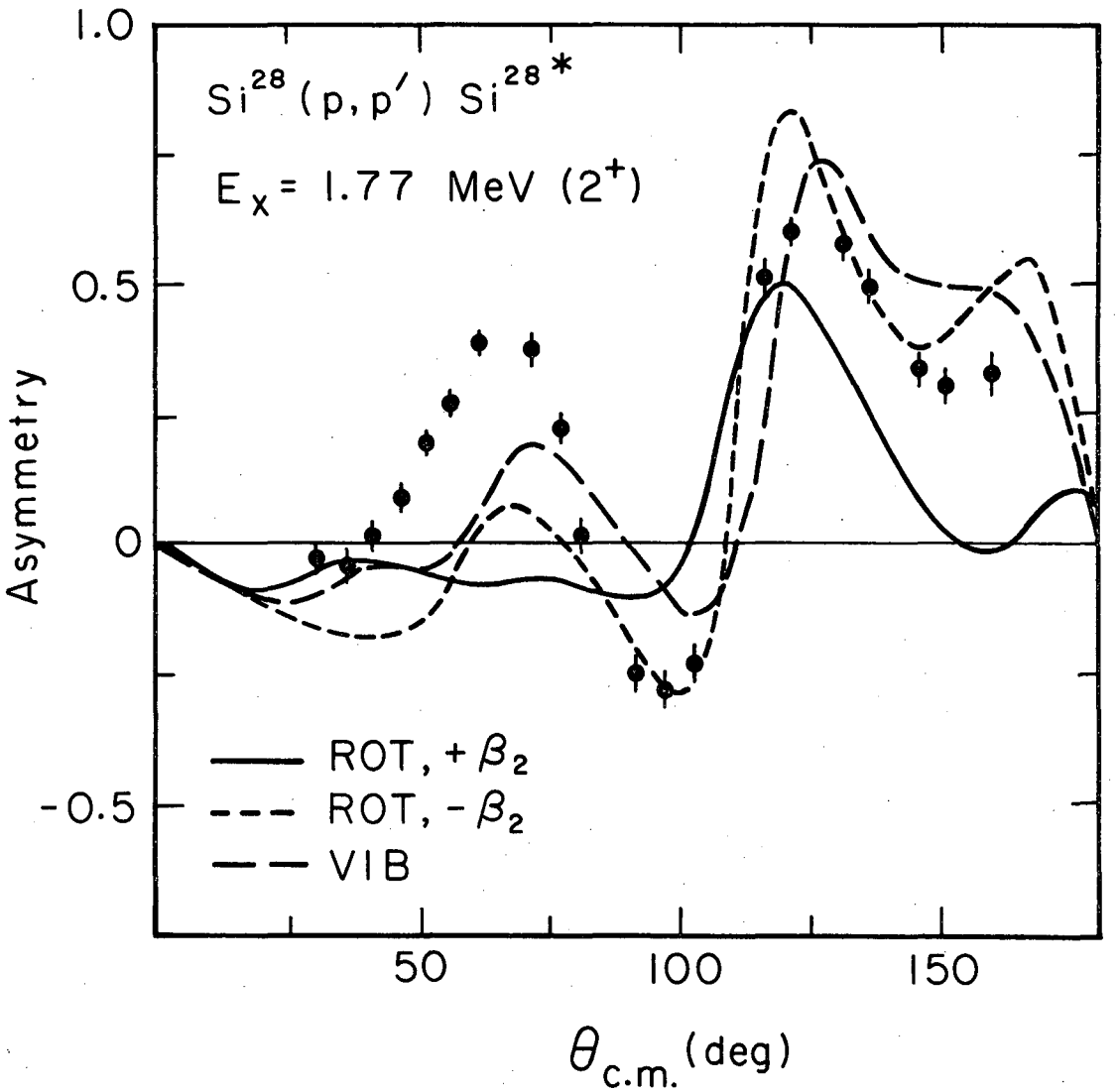


XBL695-2883

Fig. 15

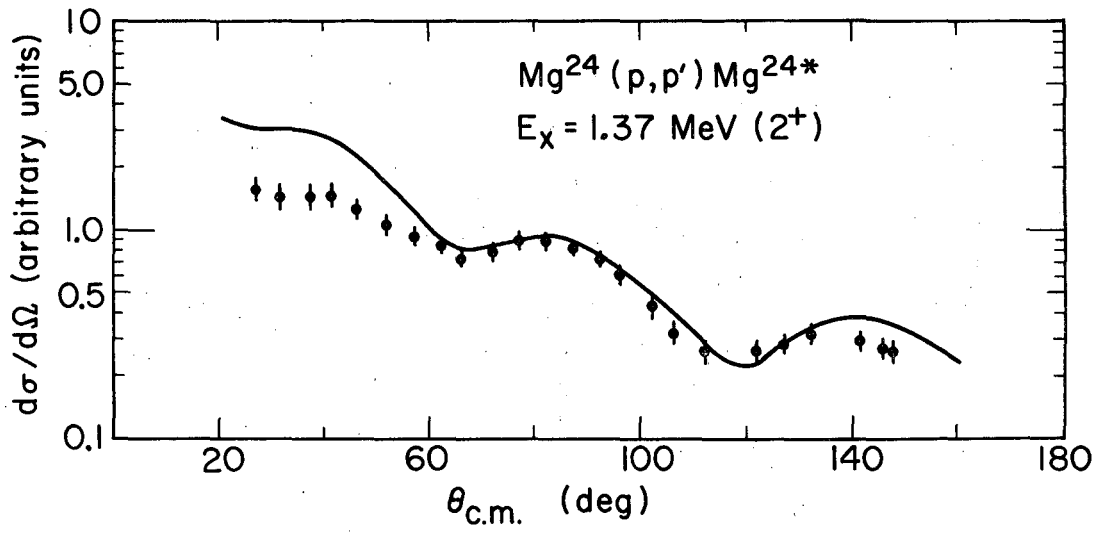


XBL697-3284

Fig. 16

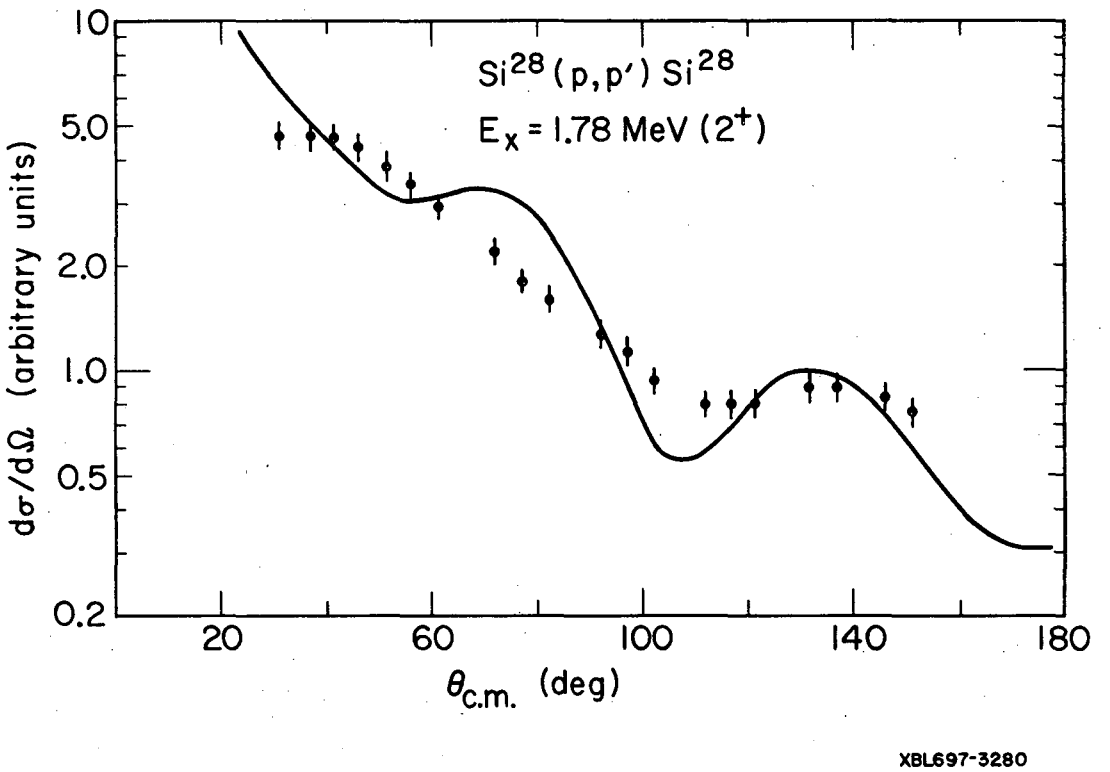
Si28 (p,p′) Si28
Ex = 1.78 MeV (2+)
dσ/dΩ (arbitrary units)
10
5.0
2.0
1.0
0.5
0.2
20
60
100
140
180
θc.m. (deg)
XBL697-3280

Fig. 17

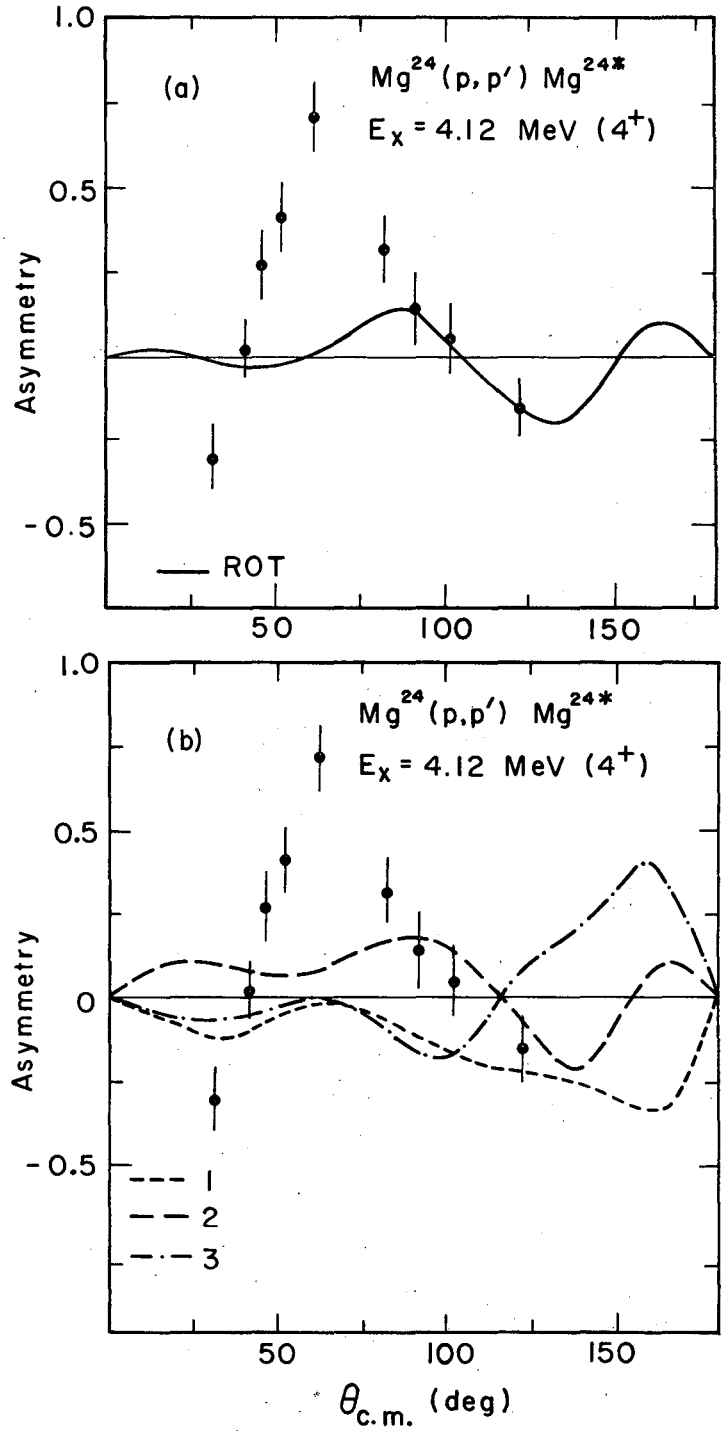


XBL 698-3491

Fig. 18

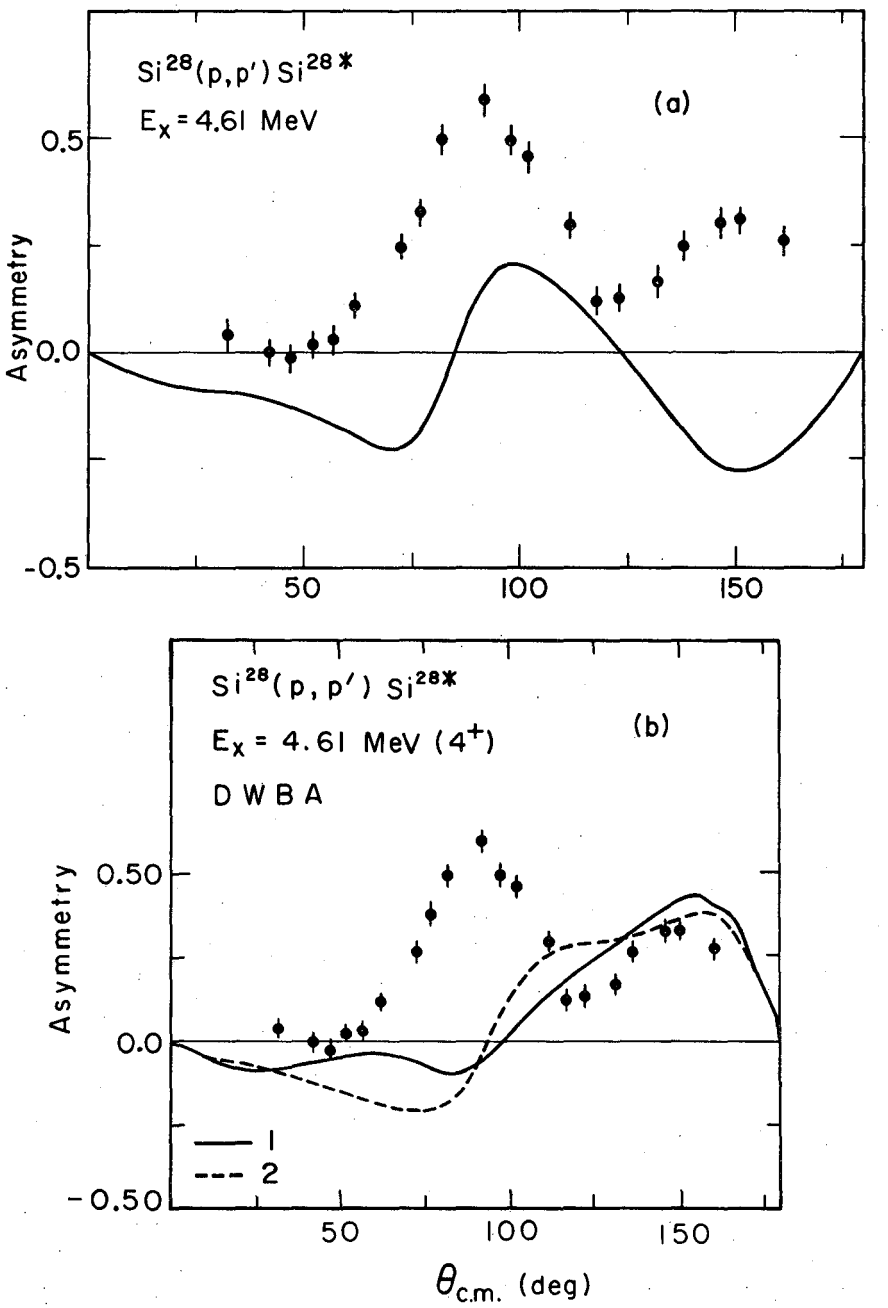


XBL698-3493

Fig. 19

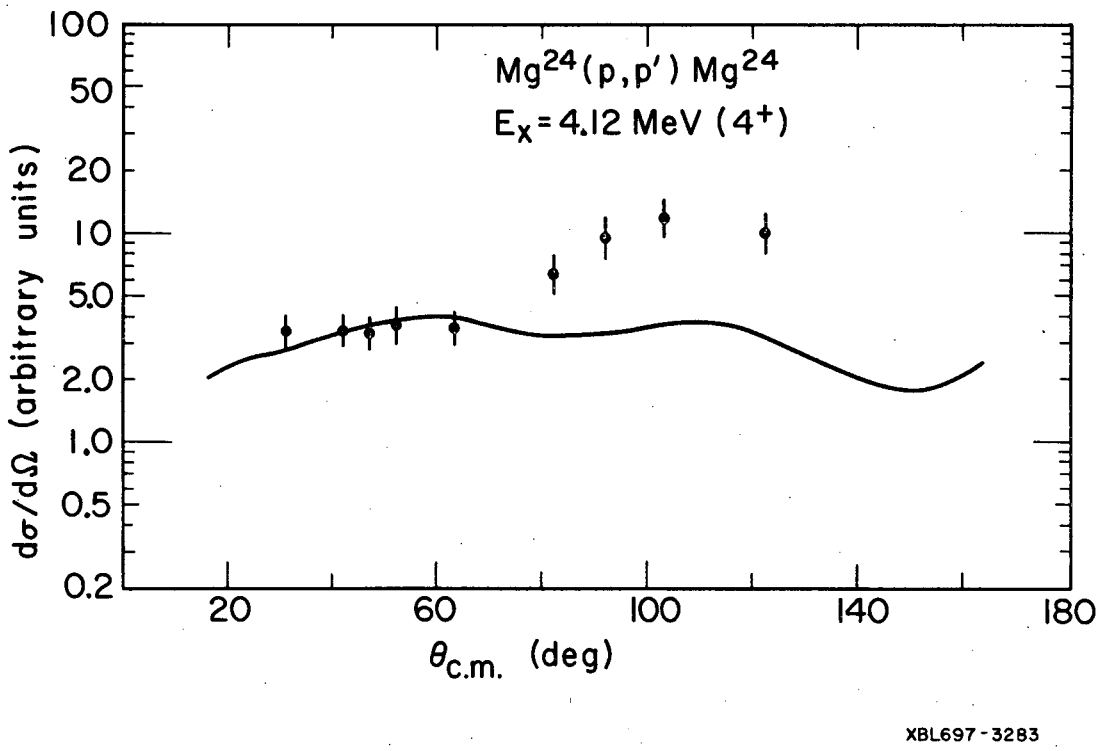
Mg24(p,p') Mg24
Ex = 4.12 MeV (4+)
dσ/dΩ (arbitrary units)
100
50
20
10
5.0
2.0
1.0
0.5
0.2
20
60
100
140
180
θc.m. (deg)
XBL697-3283

Fig. 20

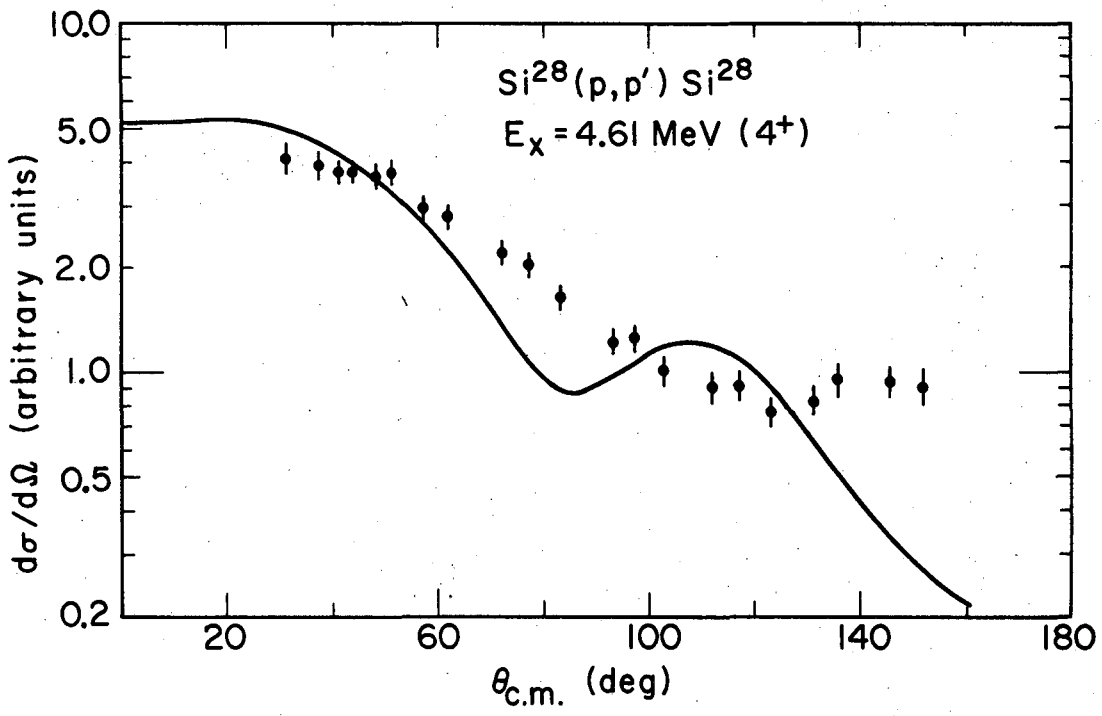


XBL697-3282

Fig. 21

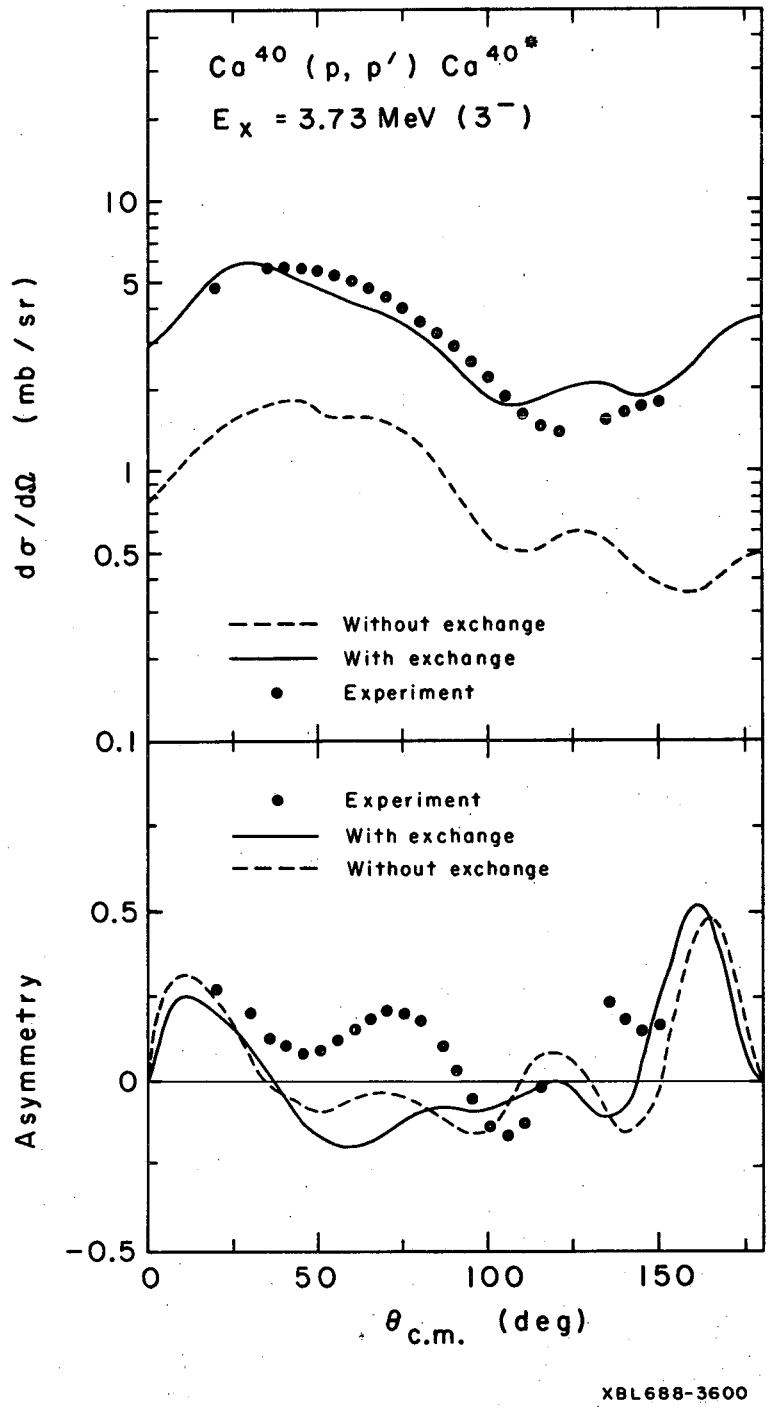
Ca 40 (p, p′) Ca 40*
E x = 3.73 MeV (3⁻)
10
5
1
0.5
0.1
dσ/dΩ (mb/sr)
Without exchange
With exchange
Experiment
Experiment
With exchange
Without exchange
0.5
0
-0.5
Asymmetry
0
50
100
150
θ c.m. (deg)
XBL688-3600

Fig. 22

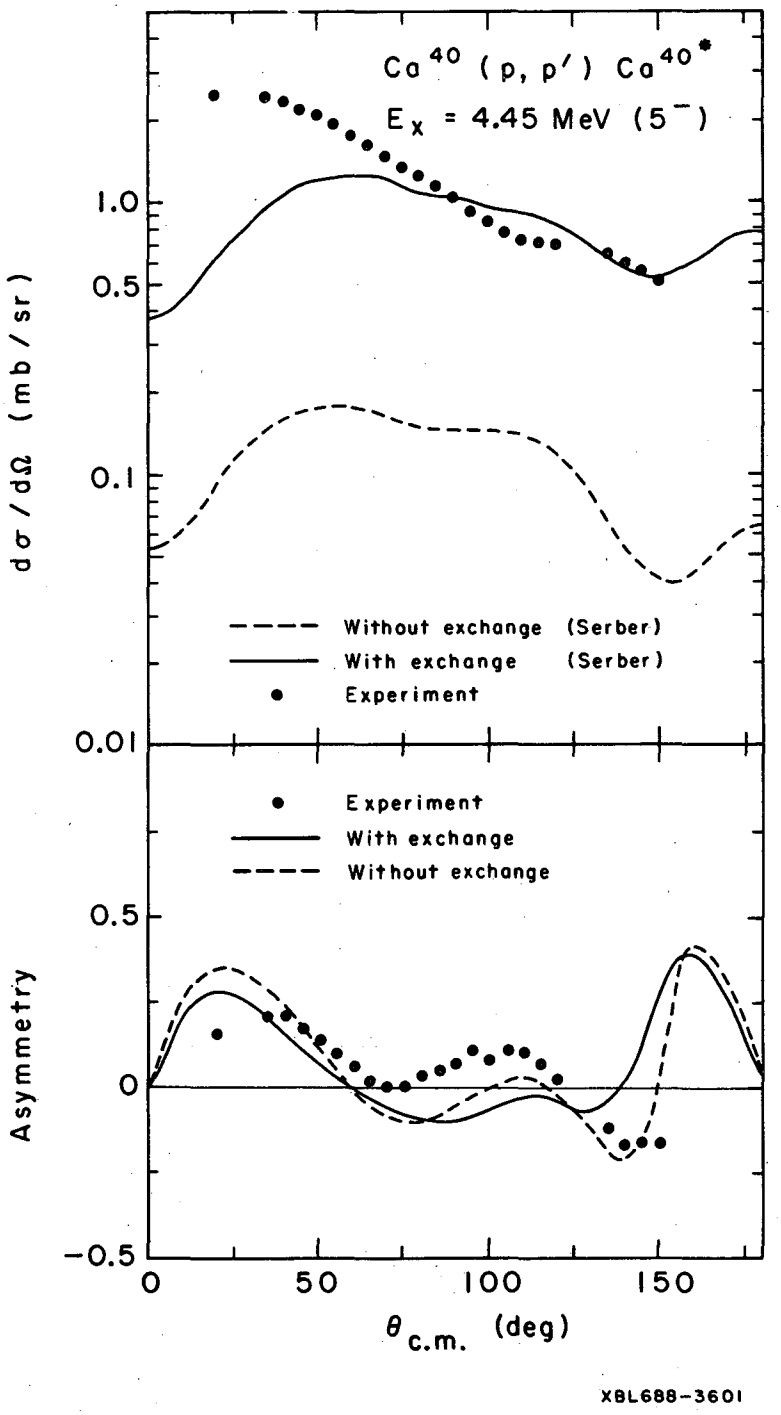
Ca 40 (p, p′) Ca 40*
Ex = 4.45 MeV (5−)
1.0
0.5
0.1
0.01
dσ / dΩ (mb / sr)
Without exchange (Serber)
With exchange (Serber)
Experiment
Experiment
With exchange
Without exchange
0.5
0
−0.5
Asymmetry
0
50
100
150
θc.m. (deg)
XBL688-3601

Fig. 23

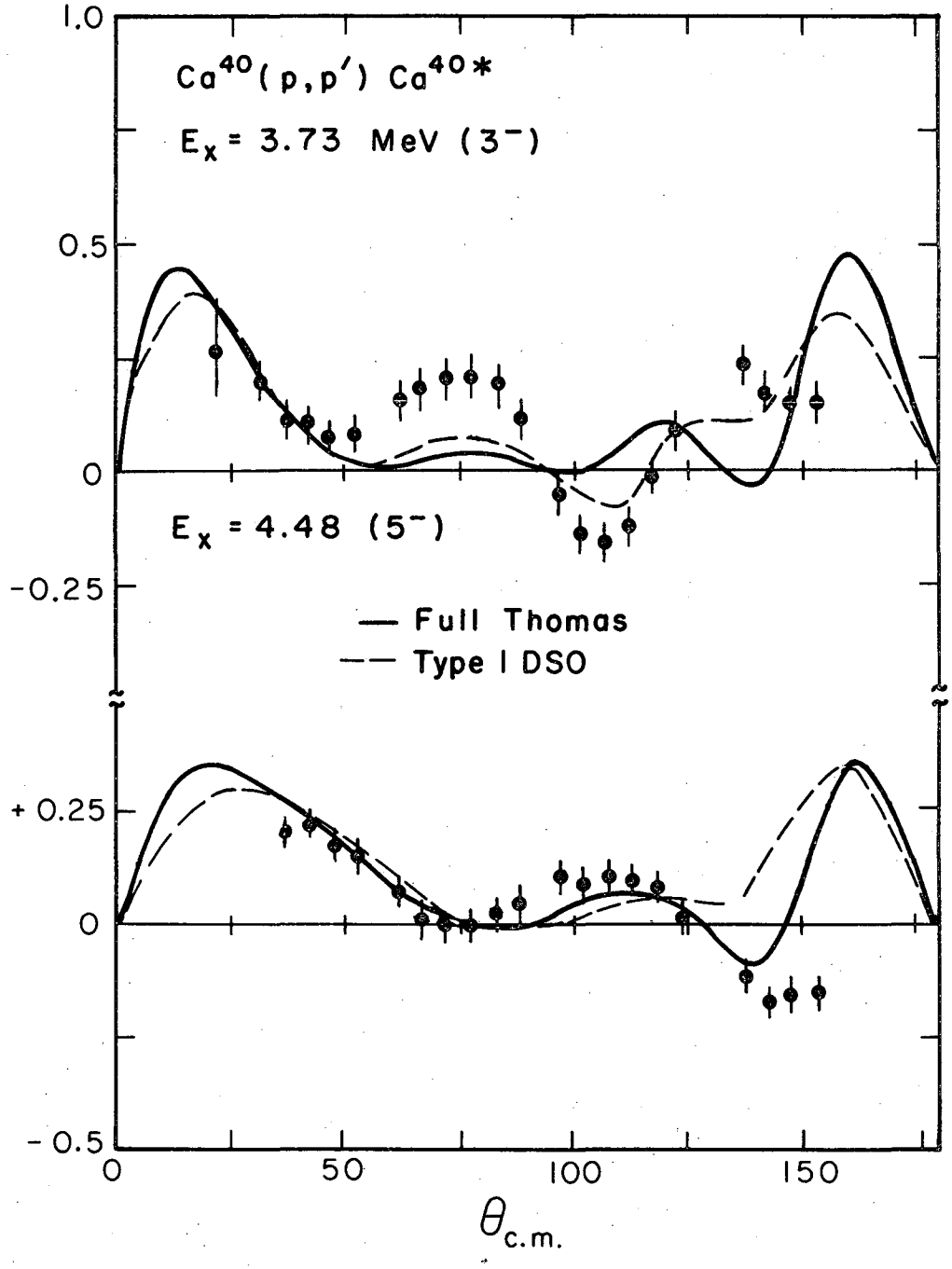


XBL 6812-7369

Fig. 24

LEGAL NOTICE

*This report was prepared as an account of Government sponsored work. Neither the United States, nor the Commission, nor any person acting on behalf of the Commission:*

*A. Makes any warranty or representation, expressed or implied, with respect to the accuracy, completeness, or usefulness of the information contained in this report, or that the use of any information, apparatus, method, or process disclosed in this report may not infringe privately owned rights; or*

*B. Assumes any liabilities with respect to the use of, or for damages resulting from the use of any information, apparatus, method, or process disclosed in this report.*

*As used in the above, "person acting on behalf of the Commission" includes any employee or contractor of the Commission, or employee of such contractor, to the extent that such employee or contractor of the Commission, or employee of such contractor prepares, disseminates, or provides access to, any information pursuant to his employment or contract with the Commission, or his employment with such contractor.*

*TECHNICAL INFORMATION DIVISION*
*LAWRENCE RADIATION LABORATORY*
*UNIVERSITY OF CALIFORNIA*
*BERKELEY, CALIFORNIA 94720*